Title: A STIM dependent dopamine-insulin axis maintains the larval drive to feed and grow in Drosophila

Authors: Nandashree Kasturacharya[1,2], Jasmine Kaur Dhall[1] and Gaiti Hasan[1,2,3]

1. National Centre for Biological Sciences, TIFR, Bellary Road, Bengaluru 560065
2. The University of Trans-Disciplinary Health Sciences and Technology (TDU), Bengaluru – 560064
3. Corresponding author: gaiti@ncbs.res.in

Abstract

Appropriate nutritional intake is essential for organismal survival. In holometabolous insects such as *Drosophila melanogaster*, the quality and quantity of food ingested as larvae determines adult size and fecundity. Here we have identified a subset of dopaminergic neurons (THD') that maintain the larval motivation to feed. Dopamine release from these neurons requires the ER Ca^{2+} sensor STIM. Larvae with loss of STIM stop feeding, whereas expression of STIM in THD' neurons rescues feeding, growth and viability of STIM null mutants. Moreover STIM is essential for maintaining excitability and release of dopamine from THD' neurons. Optogenetic stimulation of THD' neurons identified connectivity to neuropeptidergic cells, including median neuro secretory cells that secrete insulin-like peptides. Loss of STIM in THD' cells alters the developmental profile of specific insulin-like peptides including ilp3. Loss of ilp3 partially rescues STIM null mutants and inappropriate expression of ilp3 in larvae affects development and growth. In summary we have identified a novel STIM-dependent dopamine-ILP circuit that regulates developmental changes in larval feeding behaviour.

Author summary

The ability to feed appropriately when hungry is an essential feature for organismal survival and is under complex neuronal control. An array of neurotransmitters and neuropeptides integrate external and internal signalling cues to initiate, maintain and terminate feeding. In adult vertebrates and invertebrates dopamine serves as a reward cue for motor actions, including feeding. Larvae of holometabolous insects, including *Drosophila melanogaster*, feed and grow constantly followed by gradual cessation of feeding, once sufficient growth is achieved for transition to the next stages of development. Here we identified a subset of larval dopaminergic neurons in *Drosophila melanogaster*, activity in which maintains continuous feeding in larvae. By analysis of a null mutant we show that these neurons require the Stromal Interaction Molecule (STIM) an ER Ca^{2+} sensor, to maintain excitability. In turn they modulate activity of certain neuropeptidergic cells. Among these are the median neurosecretory cells

(MNSc) that synthesize and secrete insulin-like peptides including ilp3. The identified dopaminergic neurons dysregulate the normal pattern of larval ilp3 expression leading to premature cessation of feeding and growth. Overall, our study identified a simple dopamine-insulin feeding circuit whose manipulation could be useful for model organism studies related to feeding disorders, obesity and diabetes.

Introduction

Animal growth occurs primarily during the juvenile stage of development. In holometabolous insects, including *Drosophila*, larval development is considered equivalent to the juvenile stage [1]. Steady and appropriate nutritional intake in larvae, is essential for growth, and ultimately determines both survival and fecundity of the animal. In *Drosophila*, the feeding rate increases in the second instar larval stage and larvae continue to feed voraciously till the wandering stage of third instar larvae [2]. Increase in feeding rate is accompanied by acceleration of cell division and cell growth [3, 4].

Feeding behaviour and its modulation have been studied primarily in third instar larvae and adult *Drosophila,* where it is regulated by a range of neurotransmitters and neuropeptides [5]. Neuropeptide F (NPF; a human NPY homolog) serves as a signal for hunger and foraging in larvae and adults [6, 7]. Insulin like peptides (ILPs), Allatostatin A (AstA), Drosulfakinin (DSK) and Tackykinin (TK) access the internal metabolic state and terminate feeding based on the energy state of the organism [8–11]. The neuropeptide Sifamide (SifA), increases food intake in adults by integrating orexigenic and anorexigenic signals [12] whereas leukokinin (LK) regulates the frequency of meals and meal size [13]. Mutants for short Neuropeptide F (sNPF) affect body size by regulating food intake [14]. In addition serotonin and Hugin circuits support feeding and feeding-related muscle movements [15]. When food is restricted octopaminergic circuits regulate feeding independent of NPF signalling in 3rd instar larvae and in adults [16], whereas Dopaminergic circuits potentiate sugar sensitive Gustatory Receptor Neurons to consume more food [17]. Where essential amino acids are imbalanced a subset of dopaminergic neurons are required for rejection of food by larvae [18]. In adults, specific classes of Dopamine receptors signal on different neuropeptidergic cells. Dop1R1 on AstA neurons and DopEcR on DH44 cells [19] regulate different aspects of adult feeding behaviour. Multiple neuronal circuits thus integrate sensory inputs and internal metabolic state to maintain feeding and appropriate feeding behaviour in larvae and adults.

A key difference between larval and adult feeding behaviour is that adult *Drosophila* feed sporadically, driven by hunger and satiety signals [20, 21] whereas *Drosophila* larvae accelerate feeding as second instar larvae, feed continuously till the wandering stage of third instar larvae to optimise growth. They stop feeding for a few hours prior to pupariation [22,

23]. Despite studies identifying several neurotransmitters and neuropeptides in feeding regulation, neuronal circuits that maintain persistent feeding and presumably suppress the satiety signal till the wandering larval stage are not well understood. In this study, whilst characterizing the cellular and molecular phenotypes of null mutants for the ER-Calcium sensor protein STIM (**St**romal **I**nteraction **M**olecule) [24] we identified a novel dopaminergic-neuropeptide circuit that drives persistent feeding in early larvae. Growth deficits and lethality in STIM mutants appeared to have a focus in dopaminergic cells [25]. However, the cellular basis of STIM function and systemic phenotypes arising from loss of STIM in dopaminergic neurons remained to be understood. Here, we show that STIM function is required in a subset of central dopaminergic neurons for their excitability and dopamine release. These dopaminergic neurons connect to a range of neuropeptidergic cells in the central brain including the medial neurosecretory cells (MNSc) that synthesize and secrete insulin-like peptides (ilps). The dopamine-ilp circuit identified here regulates larval growth by providing the motivation for persistent larval feeding.

Results

Reduced food intake and growth deficits in STIM mutant larvae

STIM^{KO} larvae appear normal after hatching but their transition from first to second instar stages is slower than wild-type animals (**S1A and S1B Fig**) [25] and as second instars they die gradually between 86h to 326h after egg laying (**AEL; S1B Fig**). To identify the precise time window when *STIM*^{KO} larvae become sickly they were observed over 6h time intervals from 36h to 90h AEL. Whereas, wild type (*Canton-S* or CS) larvae transition from 1st to 2nd instar between 42-54h AEL, the same transition in *STIM*^{KO} larvae occurs between 60-72h AEL, indicating a delay of 18h (**Fig 1A and 1B**). The delay is followed by an inability to transition to 3rd instar (**Fig 1C**). *STIM*^{KO} larvae also exhibit retarded growth. At 72h they appear similar to CS larvae of 60h (**Fig 1D)**. After 72h however, there is a complete cessation of growth in *STIM*^{KO} larvae, followed by gradual loss of viability after 80-86h (**S1B Fig**). From these results, it became evident that cessation of growth precedes loss of viability in *STIM*^{KO} larvae.

The momentum of larval growth is maintained by constant cell division and cell growth. Normally, at the end of embryonic development, most mitotic cells such as neuroblasts (NBs) and imaginal disc cells enter a quiescent state [26]. Postembryonic larval development is initiated in the late first instar and early second instar stages by renewed cell proliferation [26,27]. Cessation of growth in *STIM*^{KO} larvae (**Fig 1D**), suggested a deficit in cell division. To investigate the status of cell proliferation in *STIM*^{KO} larvae we chose the well-characterized system of thoracic neuroblasts. Upon comparison of thoracic segments of WT and *STIM*^{KO}

109 larvae at 70-74h (**Fig 1E,** first two columns) it was evident that NBs exited from quiescence
110 and entered the proliferative state in both genotypes. Both the NB marker Deadpan (red) and
111 the post-mitotic cell marker Prospero (blue) appeared normal in *STIM*^{KO} larvae of 70-74h AEL.
112 Subsequently, at 82-86h, the number of postmitotic cells (Prospero positive) decreased
113 significantly in *STIM*^{KO} animals as compared to the controls but the number of thoracic
114 neuroblasts remained unchanged (**Fig 1E,** compare third and fourth columns). Upon
115 quantification, the ratio of dividing neuroblasts (Deadpan surrounded by Prospero positive
116 cells) to non-dividing neuroblasts (Deadpan with either no or few Prospero positive cells)
117 changed significantly in 86h aged *STIM*^{KO} larvae (**Fig 1F and 1G**). To identify the cause
118 underlying the reduced number of postmitotic cells we analyzed different phases of the cell
119 cycle of thoracic neuroblasts in *STIM*^{KO} larval brains. For this, we used the genetically encoded
120 FUCCI system [28]. Here, the G1, S, and G2 phases of interphase are marked by green, red
121 and green+red (yellow) fluorescent tags respectively. At 72-76h, both control and *STIM*^{KO}
122 showed an asynchronous pattern of division. But at 82-86h, control larvae persisted with the
123 asynchronous pattern, whereas a majority of thoracic neuroblasts in *STIM*^{KO} animals remained
124 in the G2/M state (**S1C Fig**).
125 Among other factors, the exit of quiescence and maintenance of neuroblast
126 proliferation at the early second instar stage depends on nutritional intake [29,30]. The slow
127 growth and delayed exit from quiescence suggested that *STIM*^{KO} larvae may lack adequate
128 nutritional inputs. As a first step staged larvae were placed on yeast, mixed with a blue dye
129 and tested for ingestion of food. Even as early as 40-44h AEL there was a significant reduction
130 of food intake in *STIM*^{KO} larvae (**Fig 1H,** quantification in **Fig 1I**). By 80-84h AEL two classes
131 of *STIM*^{KO} larvae were evident. One with reduced food intake and others with no food intake
132 (**Fig 1H and S1D Fig**). The proportion of *STIM*^{KO} larvae with no food intake reached ~70%
133 by 82-86h AEL (**Fig 1J**). Based on these results it appears that *STIM*^{KO} larvae gradually stop
134 feeding from early 2nd instar larvae and the consequent nutritional deficits prevent normal
135 growth.
136
137 **STIM function is required in a subset of larval dopaminergic neurons**
138 To understand how the loss of STIM might affect larval feeding we identified specific
139 cells that require STIM function for larval growth and viability. From previous work, we know
140 that knock out of *STIM* in dopaminergic neurons marked by *THGAL4* [31] leads to larval
141 lethality [25]. Over-expression of *STIM*$^{+}$ [32] in dopaminergic neurons marked by *THGAL4*
142 rescued larval lethality of *STIM*^{KO} animals to a significant extent (**S2A Fig**). Further to identify
143 specific dopaminergic neurons that require STIM function for growth and viability we tested
144 rescue by overexpression of STIM^{+} in two non-overlapping subsets of dopaminergic neurons
145 marked by *THC'GAL4* and *THD'GAL4* [33]. Rescue of *STIM*^{KO} larvae from 2nd to 3rd instar

146 (~90%) was evident upon over-expression of *STIM*$^{+}$ in THD' marked neurons (**Fig 2A and**
147 **2B**). The rescue by THD' was equivalent to the rescue by *THGAL4* (20±2 and 18±1.5 viable
148 adults respectively; **S2A Fig;** dark and light green arrows). In contrast expression of *STIM*$^{+}$ in
149 *THC'GAL4* marked neurons gave poor rescue (**5±1** adults**; S2A Fig;** blue arrow), indicating
150 that STIM function is required primarily in THD' marked dopaminergic neurons.

151 Next, we analysed *THD'* driven expression of mGFP and identified two classes of GFP
152 positive cells in the larval brain. All GFP expressing cells in the central brain (three cells of
153 DL1 and two cells of DL2 clusters [18], appear positive for Tyrosine Hydroxylase (TH) but a
154 pair of THD' cells in the ventral ganglion (VG) appear TH negative (TH^{-ve}) (**Fig 2C**). To
155 understand the relative contribution of the VG-localised TH^{-ve} cells to *THD'>STIM*$^{+}$ rescue of
156 *STIM*^{KO} animals, we restricted *THD'GAL4* expression to VG localised THD' neurons using
157 *THGAL80* [34] (**Fig 2D**). Expression of *STIM*$^{+}$ in the VG localised THD' neurons (*THD'GAL4,*
158 *THGAL80*) reduced the rescue of *STIM*^{KO} larvae significantly (**S2A Fig and Fig 2E**) and was
159 absent in adults (**Fig 2F**). Thus, the rescue of viability in *STIM*^{KO} animals derives to a significant
160 extent from brain-specific THD' dopaminergic neurons.

161 Ingestion of food is also rescued by *THD'>STIM*$^{+}$ expression in *STIM*^{KO} larvae (**Fig 2G**
162 **and 2H**). Further to confirm the relevance of STIM function in THD' marked dopaminergic
163 neurons we knocked down STIM using a previously characterized STIM RNAi (*dsSTIM*) [35].
164 *THD'>dsSTIM* animals exhibit delayed larval growth and reduced feeding (**Fig 2I-2K; S2B**
165 **Fig**) but no larval lethality. Taken together these data identified a CNS-specific subgroup of
166 dopaminergic neurons that require STIM function for persistent feeding during the early stages
167 of larval growth.

168

169 **Neuronal excitability and dopamine release requires STIM**

170 The status of THD' dopaminergic cells was investigated next in *STIM*^{KO} larval brains
171 at 80-84h, when a few viable organisms are still present despite cessation of growth and
172 feeding (**Fig 2G**). THD' cells were marked with GFP in controls, *STIM*^{KO} and *STIM*^{KO} animals
173 with STIM^{+} rescue and the brains were stained with anti-TH sera. THD'-GFP cells appeared
174 no different in *STIM*^{KO} as well as STIM^{+} rescued *STIM*^{KO} animals at 80-84h AEL when
175 compared to controls at either 58-62h or 80-84h AEL (**S3A Fig**) Moreover, the ratio of THD'
176 GFP cells to TH positive cells in the CNS also appeared identical (**S3B Fig**). Therefore, the
177 loss of STIM does not lead to the loss of dopaminergic neurons in the larval brain.

178 To understand how loss of STIM in THD' marked neurons might effect it's neuronal
179 function, we investigated their properties of excitation. For this purpose, Potassium Chloride
180 (KCl, 70mM) evoked cytosolic calcium transients were measured from THD' neurons using
181 the genetically encoded Ca^{2+} sensor GCaMP6m in *ex vivo* preparations of similarly staged
182 control (58-62h AEL) and *STIM*^{KO} (70-74h AEL) larvae. We chose these time points because

183 at 72h *STIM*^{KO} larvae appear healthy and developmentally similar to control larvae at 60h (**Fig**
184 **1D**). THD' cells responded with similar changes in GCaMP intensity, in control and *STIM*^{KO}
185 larvae at these time points (**Fig 3A-3C**). However, the ability to evoke and maintain cytosolic
186 Ca^{2+} transients upon KCl depolarisation was lost in THD' neurons of *STIM*^{KO} larvae at 76-80h
187 AEL (**Fig 3A-3C**). Overexpression of *STIM*$^{+}$ in THD' cells of *STIM*^{KO} larvae rescued the KCl
188 evoked Ca^{2+} response in larvae as late as 80-84h AEL (**Fig 3A-3C**).

189 STIM requirement for maintaining excitability of THD' neurons was tested further by
190 KCl stimulation of THD' neurons with STIM knockdown (*THD'>dsSTIM)*. Two classes of
191 responses to depolarisation by KCl were observed. A few cells (70%) responded with normal
192 or greater changes in intensity as compared to control cells, whereas in 30% of cells KCl did
193 not evoke a Ca^{2+} transient (**S3C-S3E Fig**). We attribute this heterogeneous response to
194 differential STIM knockdown by the RNAi in individual THD' cells and a potential effect of STIM
195 knock-down on ER-Ca^{2+} homeostasis (see below).

196 These data suggest that loss of STIM affects membrane excitability properties and the
197 ability of THD' neurons to respond to stimuli. This idea was tested directly by the expression
198 of transgenes that alter membrane potential. Over-expression of an inward rectifier K^{+}
199 channel, Kir2.1 in THD' neurons, that is known to hyperpolarise the plasma membrane [36],
200 resulted in developmental delays followed by the lethality of second and third instar larvae
201 (**S4A Fig**). Further, overexpression of a bacterial Na^{+} channel NaChBac [37] in THD' neurons
202 of *STIM*^{KO} larvae partially rescued developmental deficits, including the transition to third instar
203 larvae (4.4$\pm$0.4) and adult viability (2.4$\pm$0.6**; Fig. 3D-3G**). Though partial, NaChBac's rescue
204 was consistent. We attribute the variability to a stochastic effect of NaChBac in THD' cells.
205 This is also evident from the variable extent of rescue in growth observed in *STIM*^{KO};
206 *THD'>NaChBac* larvae (**Fig 3E and 3F**). Control animals with overexpression of *NaChBac* in
207 THD' neurons exhibit delayed pupariation (**S4B Fig**).

208 Neuronal excitability is required for neurotransmitter release at presynaptic terminals.
209 We hypothesized that dopamine release from THD' neurons might be affected in *STIM*^{KO}
210 larvae. To test this idea, we identified the pre-synaptic (green) and post-synaptic (red) terminal
211 regions of THD' neurons by marking them with *SyteGFP* and *Denmark* respectively (**Fig 4A)**
212 [38]**.** Analysis of pre-synaptic regions (SyteGFP expression) identified three distinct areas in
213 the CNS. One at the centre of the CNS (**Fig 4A;** asterisk), the second as a branched form
214 (**Fig 4A;** arrowhead) and the third one in the brain-gut interaction area as punctae (**Fig 4A;**
215 hash).

216 Next, dopamine release was measured in the most prominent presynaptic area of
217 THD' neurons by change in fluorescence of the genetically encoded fluorescent GPCR-
218 activation-based-DopAmine sensor (**GRAB$_{DA}$)** [39]**.** Dopamine release in THD' neurons of
219 *STIM*^{KO} larvae at 76-80h is significantly attenuated as compared with controls (**Fig 4B and**

220 **4C**). Importantly, overexpression of STIM^{+} in THD' neurons rescued dopamine release,
221 though with altered dynamics from control animals (**Fig 4B and 4C**). We chose to measure
222 dopamine release in 76-80h *STIM^{KO}* larvae because THD' neurons in their brains no longer
223 responded to KCl evoked depolarization (**Fig 3B**) even though the larvae appear normal (**Fig**
224 **1D**). Dopamine release was stimulated by Carbachol (CCh), an agonist for the muscarinic
225 acetylcholine receptor (mAChR), that links to Ca^{2+} release from ER-stores through the ER-
226 localised IP_3 receptor [40] and is expressed on THD' neurons [41]. CCh-induced changes in
227 ER-Ca^{2+} were tested directly by introducing an ER-Ca^{2+} sensor [42] in THD' neurons (**Fig 4D**
228 **and E**). Though ER-Ca^{2+} release, in response to CCh could be measured in just 7 out of 23
229 cells, the subsequent step of ER-store refilling, presumably after Store-operated Ca^{2+} entry
230 into the cytosol through the STIM/Orai pathway, could be observed in all control THD' cells
231 (58-62h AEL), whereas it was absent in THD' neurons from *STIM^{KO}* brains (76-80h AEL**; Fig**
232 **4E**). The ER-Ca^{2+} response was rescued by over-expressing STIM^{+} in THD' neurons (**Fig 4D,**
233 **and E**). Taken together our data establish an important role for STIM-dependent ER-Ca^{2+}
234 homeostasis in maintaining optimal dopamine release from THD' neurons in turn required for
235 the larval drive to feed constantly.
236 Because late third instar larvae stop feeding [2, 6, 22, 23] we hypothesized that CCh-
237 stimulated Ca^{2+} responses in THD' cells might change in wandering stage third instar larvae.
238 To test this idea we monitored carbachol-stimulated GCaMP activity in THD' neurons from
239 wild-type larvae at 96h AEL (mid 3rd instar), 120h AEL (early wandering stage) and 124h AEL
240 (late wandering stage). A robust GCaMP response was observed at 96h, whereas at the
241 beginning of the wandering stage (118-122h AEL), the peak response was both reduced and
242 delayed. A further delay in the peak response time was observed in late wandering stage
243 larvae (122-126h AEL) (**S4C and S4D Fig**). Thus with gradual cessation of feeding in late
244 third instar larvae, the dynamics of CCh-stimulated Ca^{2+} responses in THD' neurons also
245 undergo changes (see discussion).
246
247 **THD' dopaminergic neurons both activate and inhibit specific neuropeptidergic cells**
248 To understand how dopamine release modulates larval feeding we identified
249 downstream neuronal targets of THD' cells, using the *transTANGO* technique [43]. This
250 genetic tool helped identify multiple large neurons with extensive axonal projections through
251 the brain as postsynaptic partners of THD' cells (RFP fluorescence in **Fig 5A**). Spatial
252 orientation and size of the THD' postsynaptic partners suggested their identity as neuropeptide
253 cells (marked by GFP) [44, 45] in **(Fig 5B**). Connectivity between THD' cells and their
254 neuropeptidergic partners was confirmed by optogenetic stimulation of red-shifted
255 Channelrhodopsin (*CsChrimson*) [46] expressing in THD' (*THD'>UAS-Chrimson*) cells
256 followed by Ca^{2+} imaging from GCaMP6f expressing neuropeptide cells

257 *(C929LexA>LexAopGCaMP6f)* (**Fig 5C**). Upon optogenetic activation of THD' neurons, a
258 change in cellular Ca^{2+} signals was observed in a total of 64 peptidergic neurons from 9 brains,
259 including some lateral neurosecretory cells (LNCs), median neurosecretory cells (MNCs),
260 and regions of the suboesophageal ganglion (SOG) (**Fig 5C**). Elevated Ca^{2+} signals were
261 observed in a subset of neuropeptidergic cells (**Fig 5D and 5E,** yellow asterisks, n=24),
262 whereas in some cells Ca^{2+} signals were reduced (**Fig 5D and 5E,** red asterisks, n=40**)**. There
263 was no change in cellular Ca^{2+} upon optogenetic stimulation in the remaining cells with visible
264 GCaMP6f fluorescence (n=35). Upon cessation of optogenetic activation of THD' neurons
265 Ca^{2+} levels returned to baseline (**Fig 5D, 5F and 5G**). Individual cells exhibit either activatory
266 or inhibitory responses upon repeated optogenetic stimulation with pulses of red light (**S5A**
267 **and S5B Fig**), indicating that THD' cells evoke specific responses of either stimulation or
268 inhibition based on the class of neuropeptide cells. Specificity of the *THD'>Chrimson* evoked
269 response was further confirmed by testing brains from larvae that were reared without all *trans*-
270 Retinal (ATR, a cofactor for the function of Channelrhodopsin) [47] and by imaging in the
271 absence of light (**S5C Fig**). To identify dopamine receptors that might function on
272 neuropeptidergic cells we knocked down the Dop1R1 and Dop1R2 receptors using a
273 neuropeptidergic cell driver (*C929GAL4*). A delay in pupariation was observed in larvae with
274 knock down of Dop1R1 in peptidergic cells (*C929GAL4>UASDop1R1RNAi*; **S5D Fig**) but
275 larval development proceeded normally upon Dop2R2 knockdown.
276
277 **STIM expression in THD' neurons regulates the expression of insulin-like peptides**
278 Connectivity of THD' neurons and their trans-TANGO partners suggested
279 dopaminergic modulation of neuropeptidergic neurons (**Fig 5A and 5B**) by THD' cells, but did
280 not allow identification of specific neuropeptides that function downstream of the THD' neurons
281 to promote larval food intake. Optogenetic activation of THD' and Ca^{2+} responses in
282 neuropeptidergic cells (marked by *C929LexA>LexAopmCherry*) helped identify three clusters
283 of neuropeptidergic cells that are synaptically downstream of THD' neurons and include the
284 well-characterised DILP expressing MNC cluster [45], as a putative synaptic target of THD'
285 neurons (**Fig 5C and 5D**). ilp2 positive MNCs also synthesise and secrete other neuropeptide
286 including Drosulfakinin(DSK) [48]. Analysis of an RNAseq experiment, conducted
287 independently to identify changes in gene expression in brains from second instar $STIM^{KO}$
288 larvae (72-76h AEL) with developmentally comparable CS brains (58-62h;
289 https://www.ncbi.nlm.nih.gov/geo/query/acc.cgi?acc=GSE202098; to be published
290 elsewhere), found significant changes in expression of *ilp2*, *ilp3* and *ilp5*. Whereas *ilp2* and
291 *ilp5* were significantly downregulated, *ilp3* was upregulated more than 5 fold (**Fig 6A**). The
292 differential regulation of *ilp2, -3* and *-5* expression in $STIM^{KO}$ brains was further validated by
293 qPCRs (**Fig 6B**). Importantly, expression of *ilp3* and *ilp5* were restored back to normal in

294 brains from *STIM*^{KO} larvae, rescued by overexpression of *STIM*$^{+}$ in THD' neurons (**Fig 6B**).
295 During normal larval development *ilp3* transcript levels are low in actively feeding larvae (L2
296 and L3, 12h) and are gradually upregulated in later stages of L3 when larvae stop feeding (**Fig**
297 **6C**; DGET [49]). Based on the up-regulation of *ilp3* in *STIM*^{KO} larvae (**Fig 6A and 6B**), we
298 hypothesised that knock down of *ilp3* in MNSc might rescue *STIM*^{KO} larvae. Indeed, partial
299 rescue of larval lethality in 2nd instar larvae followed by their transition to 3rd instar larvae
300 (5$\pm$0.5) was observed (**Fig 6D and F**). A few of the rescued 3rd instar larvae pupariated (**Fig.**
301 **6F**, L3a type larvae) and some even eclosed as adults (2.3$\pm$0.3; **S6A and S6B Fig**). The
302 partial rescue observed may be due to lower expression of ilp2 and ilp5 in *STIM*^{KO} animals
303 because both ilps are growth signals in 2nd and 3rd instar larvae (**Fig 6A and 6B**). A small
304 proportion of *STIM*^{KO} larvae rescued by ilp3 knockdown appear significantly larger than control
305 larvae (**Fig 6F and 6G**), suggesting excess feeding in the absence of ilp3. This idea is further
306 supported by over-expression of *ilp3* in MNSc [50] where we observed smaller sized larvae
307 (**Fig 6H and 6L**), suggesting reduced feeding due to untimely over-expression of *ilp3*, and a
308 delay in larval moults from 2nd to 3rd instar stage (**Fig 6J**). Conversely, knock-down of *ilp3*
309 resulted in larger sized pupae (**Fig 6K and 6L**), suggesting prolonged feeding in 3rd instar
310 larvae, accompanied by an ~24h delay in pupariation (**Fig 6M**). Taken together, these data
311 show that loss of dopamine signals from THD' cells changes the normal expression profile of
312 *ilp3* in the MNCs and demonstrate that in normal development Ilp3 is one of the neuropeptides
313 that signals an end to larval feeding prior to pupariation.
314

315 ## Discussion

316 In *Drosophila*, as in other holometabolous insects, growth is restricted to the larval
317 stages. In early stages of larval development cells exit mitotic quiescence and re-enter mitosis
318 resulting in organismal growth [1,3,26].This change is accompanied by an increase in the
319 feeding rate of the organism so as to provide sufficient nutrition for the accompanying growth
320 in organismal size. In *STIM*^{KO} larvae we observed a loss of this ability to feed persistently
321 starting from early second instar larvae. The focus of this feeding deficit lies in a subset of
322 central dopaminergic neurons that require STIM function to maintain excitability. Importantly,
323 these dopaminergic neurons communicate with multiple neuropeptidergic cells in the brain
324 including the MNSc (**Fig 5D**) to regulate appropriate changes in larval feeding behaviour
325 through development.
326

327 **STIM and excitability of dopaminergic neurons**

328 We identified the THD' cells as critical for larval feeding from their inability to function
329 in the absence of the SOCE regulator STIM. Loss of excitability and the absence of dopamine

330 release from THD' cells in *STIM*^{KO} larvae (**Fig. 3A-3C and Fig 4B-4D**) suggests that voltage-
331 dependent receptor activity [51] is required to maintain growth in early 2nd instar larvae.
332 Changes in expression of ion channels and presynaptic components have been observed
333 earlier upon knockdown of STIM in *Drosophila* and mammalian neurons [52,53]. Moreover,
334 loss of STIM-dependent SOCE in *Drosophila* neurons effects their synaptic release properties
335 [54]. Partial rescue of viability in *STIM*^{KO} organisms by over-expression of a bacterial sodium
336 channel NaChBac (**Fig 3D-3G**) and restoration of dopamine release upon rescue by STIM^{+}
337 (**Fig. 4B and 4C**) supports the idea that STIM-dependant SOCE maybe required for
338 appropriate function and/or expression of ion channels and synaptic components in THD'
339 neurons. Changes in ER-Ca^{2+} (**Fig 4D and 5E**) suggest that STIM is also required to maintain
340 neuronal Ca^{2+} homeostasis.
341
342 **Dopaminergic control of larval food seeking**
343 Whilst mechanisms that regulate developmental progression of *Drosophila* larvae
344 have been extensively studied, neural control of essential changes in feeding behaviour that
345 need to accompany each larval developmental stage have not been identified previously.
346 Artificial manipulation of activity in the central dopaminergic neuron subset studied here
347 (THD'), either by expression of an inward rectifying potassium channel (Kir2.1) (**S4A Fig**) or
348 the bacterial sodium channel NaChBac (**S4B Fig**), suggests an important role for THD'
349 neurons during larval development. This idea is supported by the altered dynamics of
350 muscarinic acetylcholine receptor (mAChR) stimulated Ca^{2+} release observed in THD'
351 neurons between early, mid and late third instar larvae when larval feeding slows down and
352 ultimately stops (**S4C and S4D Fig**) and re-iterates that signaling in and from these neurons
353 drives larval feeding whereas lower carbachol-induced Ca^{2+} responses signal cessation of
354 feeding.
355 Though the cells that provide cholinergic inputs to THD' cells have not been identified
356 it is possible that such neurons sense the nutritional state. In this context, two pairs of cells in
357 the THD' subset also motivate the search for food in hungry adult *Drosophila* [55]. Starved
358 flies with knock down of the mAChR on THD' neurons exhibit a decrease in food seeking
359 behaviour [41]. Cholinergic inputs to THD' neurons for sensing nutritional state/hunger may
360 thus be preserved between larval and adult stages.
361 Interestingly, dopamine is also required for reward-based feeding, initiation, and
362 reinforcement of feeding behaviour in mice [56]. These findings parallel past studies where
363 mice genetically deficient for dopamine ($DA^{-/-}$), were unable to feed and died from starvation.
364 Feeding could however be initiated upon supplementation with L-DOPA [57] allowing them to
365 survive. More recent findings show that dopaminergic neurons in the ventral tegmental area

366 (VTA), and not the substantia nigra, drive motivational behaviour and facilitate action initiation
367 for feeding in mice [58].
368
369 **Dopaminergic control of neuropeptide signaling**
370 Both activation and inhibition of specific classes of neuropeptidergic cells by
371 optogenetic activation of THD' cells suggests a dual role for dopamine possibly due to the
372 presence of different classes of DA receptors. The *Drosophila* genome encodes four DA
373 receptors referred to as Dop1R1, Dop1R2, DD2R and a non-canonical DopEcR [59]. Dop1R1,
374 Dop1R2 and DopEcR activate adenylate cyclase and stimulate cAMP signaling whereas
375 DD2R is inhibitory [59]. Cell specific differences among dopamine receptors have been
376 observed in adults. Down regulation of *Dop1R1* on AstA and NPF cells shifted preference
377 towards sweet food whereas down regulation of *DopEcR* in DH44 cells shifted preference
378 towards bitter food [19]. In third instar larvae a dopaminergic-NPF circuit, arising from central
379 dopaminergic DL2 neurons, two cells of which are marked by *THD'GAL4* (**Fig 2E**), motivates
380 feeding in presence of appetitive odours [6,7]. The dopamine-neuropeptide axis identified here
381 demonstrates a broader role for dopamine in regulating neuropeptide release and/or
382 synthesis, in the context of larval feeding behaviour, perhaps similar to the mammalian circuit
383 described above.
384 Of specific interest is the untimely upregulation of *ilp3* transcripts in $STIM^{KO}$ larvae.
385 Rescue of lethality in $STIM^{KO}$ larvae either by bringing back activity to THD' neurons or by
386 reducing ilp3 levels suggests an interdependence of Dopamine-Insulin signaling that is likely
387 conserved across organisms [60–65]. Our data suggest that ilp3 expression is suppressed
388 during the feeding stages of larvae (**Fig 6H-6M**), and once enough nutrition accumulates
389 expression of ilp3 is up-regulated, concurrent with a reduction in carbachol-induced Ca^{2+}
390 signals in THD' neurons, possibly followed by release of ilp3. The idea of ilp3 as a metabolic
391 signal that is required to end persistent feeding prior to pupariation is supported by the
392 observation that knock-down of ilp3 in the MNSc leads to larger pupae in wild type animals
393 and larger larvae in $STIM^{KO}$ (**Fig 6F and G**) . To our knowledge this is the first report of ilp3
394 as a larval satiety signal. Expression of other neuropeptides did not show significant changes
395 in $STIM^{KO}$ larval brains (**S1 table**), suggesting that for neuropeptidergic cells in the LNC and
396 SOG dopamine signals alter release properties rather than synthesis. However, we were
397 unable to identify specific neuropeptides for cells in the LNC and the SOG that responded
398 upon activation of THD'.
399 The importance of dopamine for multiple aspects of feeding behaviour is well
400 documented in mice [56, 57]. Of interest are more recent findings linking dysregulation of
401 dopamine-insulin signaling with the regulation of energy metabolism [66] and the induction of
402 binge eating [67,68]. The identification of a simple neuronal circuit where dopamine-insulin

403 signaling regulates feeding could serve as a useful model for investigating new therapeutic
404 strategies targeted towards the treatment of psychological disorders for obesity and metabolic
405 syndrome [66, 67].
406

407 Material and methods

408 **Fly rearing and Stocks**:

409 *Drosophila* strains were reared on standard cornflour agar media at 25°C, unless otherwise
410 specified, under a 12:12 hr light : dark cycle. In all studies the *Canton S* (*CS*) strain was used
411 as a wild-type control and CRISPR-Cas9 generated deficiency for *STIM* referred to as $STIM^{KO}$
412 served as a null mutant for the *Drosophila STIM* gene [25]. Details of other fly lines used are
413 provided in Table 1 below.
414

415 **Staging:**

416 Synchronized larvae of the appropriate ages as described below were collected and
417 transferred to agar less media consisting of Yeast (4gm), Sucrose (8gm), cornflour (16gm),
418 Propionic acid (1ml) and 0.05gm of Benzoic acid in 1ml of absolute alcohol. These reagents
419 were mixed into 100 ml of distilled water. The number of viable organisms and the
420 developmental stage were scored at specific time points as mentioned below and in the figures
421 and figure legends.

422 Larval staging experiments were performed to obtain lethality and developmental
423 profiles of the indicated genotypes as described previously [69]. Depending on the experiment,
424 timed and synchronized egg-laying was done either for 6h to allow development profiling at
425 60-66h, 80-86h, 128-136h, 176-182h and 320-326h after egg laying or for 2h at 35-37h(36h),
426 41-43h(42h), 47-49h(48h), 53-55h(54h), 59-61h(60h), 65-67h(66h), 71-73h(72h), 83-
427 85h(84h), and 89-91h(90h) after egg laying for identifying a lethality window between 36-90h.
428 Larvae were collected at either 60–66h or 35-37h after egg laying (AEL) in batches of 25 (for
429 developmental profile) or 10 (for lethality window). They were screened and staged
430 subsequently. Heterozygous larvae were identified using dominant markers (*FM7iGFP*,
431 *TM6Tb,* and *CyOGFP*) and removed. Each batch of larvae was placed in a separate vial and
432 minimally three vials containing agar-less media were tested for every genotype at each time
433 point. The larvae were screened at the indicated time points for the number of survivors and
434 stage of development, determined by the morphology of the anterior spiracles and mouth
435 hooks(71). Experiments to determine the viability of experimental genotypes and their
436 corresponding genetic controls were performed simultaneously in all cases. Larval images
437 were taken on the MVX10 Olympus stereo microscope using an Olympus DP71 camera.
438

439 **Feeding assay:**

440 Feeding assay was performed at specific developmental time points in larvae (40-44h,
441 58-62h, 80-84h AEL) of the specified genotypes. Larvae were placed in a 35mm punched dish
442 with coverslip at the base thus creating a small depression in the centre of the coverslip. In this
443 depression a coin sized cotton swab was placed containing 4.5.% of yeast paste with 0.25%
444 eriogluasin dye (blue dye). For scoring the number of larvae that fed, 30 larvae per plate were
445 taken and incubated in the feeding plate for 4hrs at 25°C. Larvae were removed from the paste,
446 washed, collected and scored for presence of blue dye (Dye^{+ve}) and absence of blue dye
447 within the gut (Dye^{-ve}).

448 For quantification of ingested blue dye, 12-15 larvae were incubated for 2h in yeast
449 paste with the blue dye. Larvae were removed from the yeast paste and 10 larvae with blue
450 dye in the gut were washed, and homogenized in 50μl of cold 1xPBS. The homogenate was
451 spun at 5k for 2 minutes in a table top Eppendorf centrifuge. The supernatant (2μl) was taken
452 for quantification of protein using the Thermo scientific:Pierce^{TM} Protein assay kit, Cat#23227.
453 Optical density (OD) at 625nm as a measure of ingested blue dye was measured from 30μl of
454 the homogenate. Due to variation in larval sizes between control and experimental samples,
455 the OD was normalized to whole larval protein concentration (μg/μl). OD was obtained using
456 the SkanIt Software 6.1.1 RE for Microplate Readers RE, ver. 6.1.1.7. Larval imaging and
457 processing was performed on the Olympus MVX10 stereo microscope using FIJI software.

458

459 **Larval imaging and measurement:**

460 Staged larvae from specified genotypes were collected at specific development time
461 points, anesthetized on ice for 1h and mounted with ice cold HL3 buffer. The mounted larvae
462 were imaged immediately using an Olympus MVX10 stereo microscope. For measurement
463 of larval length from mouth hook to tip of the posterior spiracle FIJI software was used. A
464 minimum of 10 larvae were taken per genotype for length analysis.

465

466 **Pupal volume measurement:**

467 Pupal volume was measured by obtaining the width and height of each pupal image
468 from the Olympus MVX10 stereo microscope. A formula for obtaining the volume of a
469 cylinder, ($\pi r^2 h$) was applied to calculate the volume.

470

471 **Immunohistochemistry:**

472 Larval brains were dissected in ice-cold 1xPBS and fixed with 4% paraformaldehyde
473 in 1xPBS on the shaker for 20mins at room temperature. Fixed brains were washed with
474 PBTx (0.3% TritonX-100 in 1XPBS) 3-4 times at 10minutes intervals, blocked with 5% normal

goat serum (NGS) in PBTx for 2hrs at room temperature, and incubated with primary antibodies diluted in 5%NGS+PBTx at the appropriate concentration as mentioned below, overnight at 4°C. Antibody solution was removed and re-used upto three times. Brains were washed with PBTx 3 times at 10 minute intervals followed by incubation with secondary antibodies at the dilutions described below, for 2hrs at room temperature and three washes in PBTx of 10minute intervals each. Brains were mounted in 70% glycerol diluted in 1xPBS. Confocal images were acquired by using FV3000 LSM and the Fluoview imaging software.

Following primary antibodies were used: Chick anti-GFP (1:8000, Abcam Cat#13970 RRID: AB_300798), Rabbit anti-RFP (1:400, Rockland Immunochemicals, Inc. Cat#600-401-379; RRID: AB_2209751), Mouse anti-RFP (1:50, Rockland Immunochemicals, Inc). mouse anti-Prospero (1:100, DSHB Cat# Prospero (MR1A), RRID:AB_528440), Rabbit anti-Deadpan (1:400, Abcam– ab195172), Mouse anti-TH (1:5, ImmunoStar Cat#22941; RRID: AB_572268), Mouse anti-bruchpilot (NC82) (dilution1:50, monoclonal, Gift from Eric Buchner, University of Wuerzburg, Germany).

Following secondary antibodies were used :Goat anti-Chicken IgY (H+L), Alexa Fluor 488 (Thermo Fischer Scientific, Cat#A-11039; RRID: AB_2534096), Goat anti-Rabbit IgG (H+L), Alexa Fluor 568(Thermo Fischer Scientific Cat# A-11011; RRID: AB_143157), Goat anti-Mouse IgG (H+L) Alexa Fluor 633 (Thermo Fischer Scientific Cat# A-21052; RRID: AB_2535719), Goat anti-Rabbit IgG (H+L) Alexa Fluor 594 (Thermo Fischer Scientific Cat#A-11037; RRID: AB_2534095).

Ex-vivo imaging of the larval brain:

GCaMP signals were obtained from appropriately aged larval brains dissected from the specified genotypes and dissected in hemolymph like saline (HL3) (70mM NaCl, 5mM KCl, 20mM MgCl2, 10mM NaHCO3, 5mM trehalose, 115mM sucrose, 5 mM HEPES, 1.5mM Ca2+, pH 7.2). Dissected brains were transferred to a 35mm punched dish with a cover slip adhered to the bottom. Brains were embedded in ~5μl of 0.8% low melt agarose (Invitrogen, Cat#16520-100) and bathed in 86μl of HL3. Images were acquired as a time series on an XY plane at an interval of 2sec using a 20X-oil objective on an Olympus FV3000 inverted confocal microscope (Olympus Corp., Japan). For KCl stimulation, at the 40th frame, 7μl of HL3 was added and at the 80th frame 7μl of 1M KCl was added. The final concentration of KCl in the solution surrounding the brain was 70mM. For stimulation with Carbachol (Sigma Aldrich Cat# C4382), 10μl of HL3 was added at the 40th frame followed by 10μl of 100mM Carbachol at the 80th frame. Final carbachol concentration was maintained at 0.5mM Ca^{2+} responses were imaged till the 300th frame (600sec).

510 Changes in ER-Ca^{2+} were measured using an ER-GCaMP-210 strain(42). The brain
511 sample was prepared as above. Images were acquired as a time series on an XY plane at an
512 interval of 1 sec using a 20X oil objective on an Olympus FV3000 inverted confocal microscope
513 (Olympus Corp., Japan). For Carbachol stimulation, 10μl of HL3 was added at the 50th frame
514 and 10μl of 100mM of Carbachol was added at the 100th frame. Final carbachol concentration
515 was maintained at 0.5mM. Images were obtained for 600 frames (600 secs).
516
517 **Analysis of Optogenetic signals:**
518 Larvae from the specified genotypes were reared in fly media containing 0.2mM ATR
519 (All-trans retinal Sigma-Aldrich Cat#R2500). Brain samples were prepared as mentioned
520 above. Images were acquired as a time series on an XY plane at an interval of 2 sec/frame
521 using a 20X oil objective on an Olympus FV3000 inverted confocal microscope (Olympus
522 Corp., Japan). For optogenetic stimulation of *CsChrimson*, a 633nm LED (from Thor labs) was
523 used and GCaMP6f fluorescent images were obtained simultaneously using a 488nm laser
524 line so as to measure changes in cytosolic Ca^{2+} upon CsChrimson activation. Image acquired
525 till 200th frames (400 secs).
526 A minimum of 6 independent brain preparations were used for all live imaging
527 experiments and the exact number of cells imaged are indicated in the figures. Raw
528 fluorescence data were extracted from the marked ROIs using a time series analyzer plugin in
529 Fiji. ΔF/F was calculated using the following formula for each time point (t): $\Delta F/F = (F_t/F_0)/F_0$,
530 where F_0 is the average basal fluorescence obtained from the first 40 frames.
531
532 **RNA isolation and quantitative PCR**
533 Larval brains from appropriate genotypes and their respective age were dissected in
534 ice cold 1XPBS. Larval brains (10-15) were transferred to a microtube containing 500µl TRIzol
535 (Life Technologies), and vortexed immediately for 10-15secs. After vortexing the samples
536 were either processed within 30 min or stored at −80 °C for processing for up to 2 weeks. RNA
537 was isolated following manufacturer's protocol for TRIzol. Concentration and integrity of RNA
538 was determined on a bioanalyzer (Agilent 2100). RNA (1μg) was taken for cDNA synthesis.
539 DNAse treatment and first strand synthesis was performed as previously described [70].
540 Reverse Transcription followed by PCR (RT-PCR) was performed in a reaction mixture of 25
541 µl with 1 µl of the cDNA. Quantitative real time PCRs (qPCRs) were performed in a total volume
542 of 10µl with Kapa SYBR Fast qPCR kit (KAPA Biosystems) on a QuantStudio™ 3 Real-Time
543 PCR system. Duplicates were performed for each qPCR reaction. Minimum of three biological
544 replicates were taken for each qPCR reaction. *rp49* was used as the internal control. The fold

545 change of gene expression in any experimental condition relative to wild-type was calculated
546 as $2^{-\Delta\Delta Ct}$, where $\Delta\Delta Ct = (Ct\ (target\ gene) - Ct\ (rp49))_{Expt.} - (Ct\ (target\ gene) - Ct\ (rp49))_{Control.}$
547
548 Sequences of PCR primers used are as follows:
549 ***rp49***
550 F_5'CGGATCGATATGCTAAGCTGT3'
551 R_5'GCGCTTGTTCGATCCGTA3'
552 ***dilp2***
553 F_5'CCATGAGCAAGCCTTTGTCC3'
554 R_5'TTCACTGCAGAGCGTTCCTTG3'
555 ***dilp3***
556 F_5'ACTCGACGTCTTCGGGATG3'
557 R_5'CGAGGTTTACGTTCTCGGCT3'
558 ***dilp5***
559 F_5'ACTCACTGTCGAGCATTCGG3'
560 R_5'GAGTCGCAGTATGCCCTCAA3'
561
562 **Quantification and Statistical Analysis**
563 All bar graphs and line plots show the means and standard error of means. In boxplots,
564 horizontal lines in the box indicate median, box limits are from 25th-75th percentiles, and
565 individual data points are represented by closed circles (unless otherwise specified in the figure
566 legends). Unpaired student t-Test is done to calculate the P value. All graphs were plotted
567 using Origin 8.0 software. Origin 7.5 MicroCal, Origin Lab, Northampton, MA, USA N/A, Fiji
568 Open access (RRID:SCR_002285).
569
570 **Table 1: Fly strains**

Fly line	Description	Source
Canton S	Wild type	
STIM^{KO}	Null mutant for STIM gene generated with help of CRISPR-Cas9 gene editing technique	Generated in the lab
THGAL4	Dopaminergic GAL4 driver marks TH (Tyrosine Hydroxylase) positive cells in brain and hypoderma	Serge Birman CNRS, ESPCI Paris Tech, France

THGAL80	Inhibits Gal4 expression in Dopaminergic cells	Toshihiro Kitamoto, University of Iowa, Carver College of Medicine.
THD'GAL4	Marks subgroup of Dopaminergic cells in larval brain	Mark N Wu, Johns Hopkins University, Baltimore
THC'GAL4	Marks dopaminergic cells of larval brain	
C929GAL4	Marks neuropeptidergic cells	P. H. Taghert, Washington University
c929LexA (DimmLexA)	Marks neuropeptidergic cells	Michael Texada, Janelia Farms, USA
transTango	Marks Post synaptic neurons with RFP	Michael Rosbash, Brandeis University, USA
UASSTIM+	*Stim* wildtype cDNA under UAS control	Generated in the lab
UASGRAB$_{DA}$	A Genetically Encoded Fluorescent Sensor for Dopamine	Yulong Li, Peking University School of Life Sciences, Beijing, China
LexAopmCherry	Expresses mCherry under LexAop control	Claude Desplan, New York University, USA
UASmCD8GFP	Expresses membrane tagged GFP under UAS control	RRID: BDSC_5130
UASKir2.1	Prevents membrane depolarization	RRID: BDSC_6595
UASGCaMP6m	Ca^{2+} Sensor with intermediate kinetics expresses under UAS	RRID: BDSC_42748 from Douglas Kim
LexAopGCaMP6f	Ca^{2+} Sensor with faster kinetics expresses under LexAop	RRID: BDSC_44277

UASSyteGFP,Denmark	Syt-GFP marks presynaptic terminal and Denmark (RFP) marks post synaptic part of the neuron.	RRID: BDSC_33065
UASCsChrimson	Optogenetically encoded cation channel that is activated at 625nm	RRID: BDSC_55136
InscGAL4	Marks neuroblasts of larval brain with GAL4	RRID: BDSC_8751
UASFUCCI	Marks different phases of cell cycle with fluorescent markers	RRID: BDSC_55100
UASNaChBac	Increases sodium conductance and therefore activates the neuron	RRID: BDSC_9468
UASERGCaMP-210	ER specific Ca^{2+} sensor	Cahir O'Kane, Cambridge University, UK
dsSTIM (III)	UAS-RNAi against Stim gene	VDRC_47073
UASDicer2(X)	Enhancer for RNAi	RRID: BDSC_24648
Dilp2GAL4	Marks ilp producing MNSc cells of larval brain	RRID: BDSC_37516
UASilp3^{+}	Over expression of wildtype ilp3 gene	Ernst Hafen's lab
UASdsilp3	RNAi for ilp3 gene	RRID: BDSC_33681
UASDop1R1RNAi	RNAi for Dop1R1 receptor	RRID: BDSC_62193
THD'GAL4, THGAL80/CyO	Recombinant line made for this study	
THD'GAL4, UASGCaMP6m/CyO		
c929LexA, LexAopGCaMP6f, LexAopmCherry/TM6Tb		
THD'GAL4, UASCsChrimson/CyO		

STIM^{KO}; +; THGAL4/TM3SerG	Strains made for this study
STIM^{KO}; THD'GAL4/CyOG	
STIM^{KO}; THC'GAL4/CyOG	
STIM^{KO}; UASSTIM/CyOG	
STIM^{KO}; UASGCaMP6m/CyOG	
STIM^{KO}; UASmCD8GFP/CyOG	
STIM^{KO}; UASdsilp3/CyOG	
STIM^{KO}; UASMNScGAL4/CyOG	
UAS-STIM+; UASGRAB$_{DA}$	
UAS-STIM+; UASERGCaMP-210	

Acknowledgements

This study was supported by core funds from NCBS (TIFR), a SERB distinguished fellowship to GH (SB/S9/YSCP/SERB-DF/2018-1) and a DST-WOS-A grant (SR/WOS-A/LS-703/2016) to NK. We thank Fly Facility at NCBS for fly lines and NCBS Central Imaging and Flow Facility (CIFF) for confocal imaging and NCBS lab support for timely help.

References:

1. Tennessen JM, Thummel CS. Coordinating growth and maturation - Insights from Drosophila. Curr Biol. 2011;21: R750–757. PMID: 21959165
2. Sewell D, Burnet B, Connolly K. Genetic analysis of larval feeding behaviour in Drosophila melanogaster. Genet. Res. 1974;24: 163–173. PMID: 4217753
3. Colombani J, Raisin S, Pantalacci S, Radimerski T, Montagne J, Léopold P. A Nutrient Sensor Mechanism Controls Drosophila Growth. Cell. 2003 ;114: 739–749. PMID: 14505573
4. Layalle S, Arquier N, Léopold P. The TOR Pathway Couples Nutrition and Developmental Timing in Drosophila. Dev Cell. 2008;15: 568–77. PMID: 18854141
5. Nässel DR, Zandawala M. Hormonal axes in Drosophila: regulation of hormone release and multiplicity of actions. Cell Tissue Res. 2020;382: 233–266. PMID: 32827072

590 6. Wu Q, Wen T, Lee G, Park JH, Cai HN, Shen P. Developmental Control of Foraging and
591 Social Behavior by the Drosophila Neuropeptide Y-like System. Neuron. 2003;39: 147–
592 161. PMID: 12848939
593 7. Pu Y, Zhang Y, Zhang Y, Shen P. Two Drosophila Neuropeptide Y-like Neurons Define a
594 Reward Module for Transforming Appetitive Odor Representations to Motivation. Sci Rep.
595 2018;8: 11658. PMID: 30076343
596 8. Erion R, Sehgal A. Regulation of insect behavior via the insulin-signaling pathway. Front
597 Physiol. 2013;4: 1–6. PMID: 24348428
598 9. Guo D, Zhang YJ, Zhang S, Li J, Guo C, Pan YF, et al. Cholecystokinin-like peptide
599 mediates satiety by inhibiting sugar attraction. PLoS Genet. 2021;17(8): e1009724.
600 PMID: 34398892
601 10. Hergarden AC, Tayler TD, Anderson DJ. Allatostatin-A neurons inhibit feeding behavior
602 in adult Drosophila. Proc Natl Acad Sci U S A. 2012;109: 3967–372. PMID: 22345563
603 11. Qi W, Wang G, Wang L. A novel satiety sensor detects circulating glucose and
604 suppresses food consumption via insulin-producing cells in Drosophila. Cell Res.
605 2021;31: 580–8. PMID: 33273704
606 12. Martelli C, Pech U, Kobbenbring S, Pauls D, Bahl B, Sommer MV, et al. SIFamide
607 Translates Hunger Signals into Appetitive and Feeding Behavior in Drosophila. Cell Rep.
608 2017;20: 464–78. PMID: 28700946
609 13. Al-Anzi B, Armand E, Nagamei P, Olszewski M, Sapin V, Waters C, et al. The leucokinin
610 pathway and its neurons regulate meal size in Drosophila. Curr Biol. 2010;20: 969–78.
611 PMID: 20493701
612 14. Lee KS, You KH, Choo JK, Han YM, Yu K. Drosophila short neuropeptide F regulates
613 food intake and body size. J Biol Chem. 2004;279: 50781–50789. PMID: 15385546
614 15. Schoofs A, Hückesfeld S, Pankratz MJ. Serotonergic network in the subesophageal zone
615 modulates the motor pattern for food intake in Drosophila. J Insect Physiol. 2018;106:36–
616 46. PMID: 28735009
617 16. Youn H, Kirkhart C, Chia J, Scott K. A subset of octopaminergic neurons that promotes
618 feeding initiation in Drosophila melanogaster. PLoS One. 2018;13: e0198362.
619 PMID: 29949586
620 17. Inagaki HK, Ben-Tabou De-Leon S, Wong AM, Jagadish S, Ishimoto H, Barnea G, et al.
621 Visualizing neuromodulation in vivo: TANGO-mapping of dopamine signaling reveals
622 appetite control of sugar sensing. Cell. 2012;148: 583–95. PMID: 22304923
623 18. Bjordal M, Arquier N, Kniazeff J, Pin JP, Léopold P. Sensing of Amino Acids in a
624 Dopaminergic Circuitry Promotes Rejection of an Incomplete Diet in Drosophila. Cell.
625 2014;156: 510–521. PMID: 24485457

626 19. Sareen PF, McCurdy LY, Nitabach MN. A neuronal ensemble encoding adaptive choice
627 during sensory conflict in Drosophila. Nat Commun. 2021;12: 4131. PMID: 34226544
628 20. Ahima RS, Antwi DA. Brain Regulation of Appetite and Satiety. Endocrinol Metab Clin
629 North Am. 2008;37: 811–823.
630 21. Lin S, Senapati B, Tsao CH. Neural basis of hunger-driven behaviour in Drosophila. Open
631 Biol. 2019;9. PMID: 30914005
632 22. Almeida de Carvalho MJ, Mirth CK. Food intake and food choice are altered by the
633 developmental transition at critical weight in Drosophila melanogaster. Anim Behav.
634 2017;126: 195–208.
635 23. Wegman LJ, Ainsley JA, Johnson WA. Developmental timing of a sensory-mediated larval
636 surfacing behavior correlates with cessation of feeding and determination of final adult
637 size. Dev Biol. 2010;345: 170–179. PMID: 20630480
638 24. Zhang SL, Yu Y, Roos J, Kozak JA, Deerinck TJ, Ellisman MH, et al. STIM1 is a Ca2+
639 sensor that activates CRAC channels and migrates from the Ca2+ store to the plasma
640 membrane. Nature. 2005;437: 902–905. PMID: 16208375
641 25. Pathak T, Trivedi D, Hasan G. CRISPR-Cas-Induced Mutants Identify a Requirement for
642 dSTIM in Larval Dopaminergic Cells of *Drosophila melanogaster*. G3. 2017;7: 923–933.
643 PMID: 28131984
644 26. Doe CQ. Neural stem cells: balancing self-renewal with differentiation. Development.
645 2008;135: 1575–1587. PMID: 18356248
646 27. Spéder P, Brand AH. Systemic and local cues drive neural stem cell niche remodelling
647 during neurogenesis in Drosophila. Elife. 2018;7: 1–16. PMID: 29299997
648 28. Zielke N, Korzelius J, Straaten M Van, Bender K, Schuhknecht GFP, Dutta D, et al.
649 Resource Fly-FUCCI : A Versatile Tool for Studying Cell Proliferation in Complex Tissues.
650 Cell Rep. 2014;7: 588–598. PMID: 24726363
651 29. Britton JS, Edgar BA. Environmental control of the cell cycle in Drosophila: Nutrition
652 activates mitotic and endoreplicative cells by distinct mechanisms. Development.
653 1998;125: 2149–2158. PMID: 9570778
654 30. Sousa-Nunes R, Cheng LY, Gould AP. Regulating neural proliferation in the Drosophila
655 CNS. Curr Opin Neurobiol. 2010;20: 50–57. PMID: 20079625
656 31. Friggi-Grelin F, Coulom H, Meller M, Gomez D, Hirsh J, Birman S. Targeted gene
657 expression in Drosophila dopaminergic cells using regulatory sequences from tyrosine
658 hydroxylase. J Neurobiol. 2003;54: 618–627. PMID: 12555273
659 32. Agrawal N, Venkiteswaran G, Sadaf S, Padmanabhan N, Banerjee S, Hasan G. Inositol
660 1,4,5-trisphosphate receptor and dSTIM function in Drosophila insulin-producing neurons
661 regulates systemic intracellular calcium homeostasis and flight. J Neurosci. 2010;30:
662 1301–1313. PMID: 20107057

663 33. Liu Q, Liu S, Kodama L, Driscoll MR, Wu MN. Two dopaminergic neurons signal to the
664 dorsal fan-shaped body to promote wakefulness in Drosophila. Curr Biol. 2012;22: 2114–
665 2123. PMID: 23022067
666 34. Sitaraman D, Zars M, LaFerriere H, Chen YC, Sable-Smith A, Kitamoto T, et al. Serotonin
667 is necessary for place memory in *Drosophila*. Proc Natl Acad Sci U S A. 2008;105: 5579–
668 5584 PMID: 18385379
669 35. Venkiteswaran G, Hasan G. Intracellular Ca2+ signaling and store-operated Ca2+ entry
670 are required in Drosophila neurons for flight. Proc Natl Acad Sci U S A. 2009;106: 10326–
671 10331. PMID: 19515818
672 36. Nitabach MN, Blau J, Holmes TC. Electrical Silencing of Drosophila Pacemaker Neurons
673 Stops the Free-Running Circadian Clock An important area of circadian rhythm research
674 is the relationship between the function of the molecular clock in pacemaker neurons and
675 the central physiological. Cell. 2002; 109: 485–495. PMID: 12086605
676 37. Nitabach MN, Wu Y, Sheeba V, Lemon WC, Strumbos J, Zelensky PK, et al. Electrical
677 hyperexcitation of lateral ventral pacemaker neurons desynchronizes downstream
678 circadian oscillators in the fly circadian circuit and induces multiple behavioral periods. J
679 Neurosci. 2006;26: 479–489. PMID: 16407545
680 38. Nicolaï LJJ, Ramaekers A, Raemaekers T, Drozdzecki A, Mauss AS, Yan J, et al.
681 Genetically encoded dendritic marker sheds light on neuronal connectivity in Drosophila.
682 Proc Natl Acad Sci U S A. 2010;107: 20553–20558. PMID: 21059961
683 39. Sun F, Zeng J, Jing M, Zhou J, Feng J, Owen SF, et al. A Genetically Encoded
684 Fluorescent Sensor Enables Rapid and Specific Detection of Dopamine in Flies, Fish, and
685 Mice. Cell. 2018;174: 481-496.e19. PMID: 30007419
686 40. Luo D, Broad LM, Bird GSJ, Putney JW. Signaling Pathways Underlying Muscarinic
687 Receptor-induced [Ca 2+]i Oscillations in HEK293 Cells. J Biol Chem. 2001;276: 5613–
688 5621. PMID: 11096083
689 41. Sharma A, Hasan G. Modulation of flight and feeding behaviours requires presynaptic
690 IP3Rs in dopaminergic neurons. Elife. 2020;9: 1–25. PMID: 33155978
691 42. Oliva MK, Pérez-Moreno JJ, O'Shaughnessy J, Wardill TJ, O'Kane CJ. Endoplasmic
692 Reticulum Lumenal Indicators in Drosophila Reveal Effects of HSP-Related Mutations on
693 Endoplasmic Reticulum Calcium Dynamics. Front Neurosci. 2020;14: 1–10.
694 PMID: 32903680
695 43. Talay M, Richman EB, Snell NJ, Hartmann GG, Fisher JD, Sorkaç A, et al. Transsynaptic
696 Mapping of Second-Order Taste Neurons in Flies by trans-Tango. Neuron. 2017;96: 783-
697 795.e4. PMID: 29107518
698 44. Park D, Veenstra JA, Park JH, Taghert PH. Mapping peptidergic cells in Drosophila:
699 Where DIMM fits in. PLoS One. 2008;3(3). PMID: 18365028

45. Nässel DR, Zandawala M. Recent advances in neuropeptide signaling in Drosophila, from genes to physiology and behavior. Prog Neurobiol. Elsevier Ltd; 2019;179. PMID: 30905728
46. Klapoetke NC, Murata Y, Kim SS, Pulver SR, Birdsey-Benson A, Cho YK, et al. Independent optical excitation of distinct neural populations. Nat Methods. 2014;11: 338–346. PMID: 24509633
47. Fenno L, Yizhar O, Deisseroth K. The Development and Application of Optogenetics. Annu Rev Neurosci 2011;34: 389–412. PMID: 21692661
48. Söderberg JAE, Carlsson MA, Nässel DR. Insulin-Producing Cells in the Drosophila Brain also Express Satiety-Inducing Cholecystokinin-Like Peptide, Drosulfakinin. Front Endocrinol (Lausanne). 2012;3. PMID: 22969751
49. Hu Y, Comjean A, Perrimon N, Mohr SE. The Drosophila Gene Expression Tool (DGET) for expression analyses. BMC Bioinformatics. 2017;18. PMID: 28187709
50. Rulifson EJ, Kim SK, Nusse R. Ablation of Insulin-Producing Neurons in Flies: Growth and Diabetic Phenotypes. Science. 2002;296:1118–1120. PMID: 1200413
51. Rozenfeld E, Tauber M, Ben-Chaim Y, Parnas M. GPCR voltage dependence controls neuronal plasticity and behavior. Nat Commun. 2021;12: 7252. PMID: 34903750
52. Mitra R, Hasan G. Store-operated Ca2+ entry regulates neuronal gene expression and function. Curr Opin Neurobiol. 2022;73: 102520. PMID: 35220059
53. Dhanya SK, Hasan G. Purkinje Neurons with Loss of STIM1 Exhibit Age-Dependent Changes in Gene Expression and Synaptic Components. J Neurosci. 2022;41(17): 3777–3798. PMID: 33737457
54. Richhariya S, Jayakumar S, Abruzzi K, Rosbash M, Hasan G. A pupal transcriptomic screen identifies Ral as a target of store-operated calcium entry in Drosophila neurons. Sci Rep. 2017;7: 1–12. PMID: 28195208
55. Tsao CH, Chen CC, Lin CH, Yang HY, Lin S. Drosophila mushroom bodies integrate hunger and satiety signals to control innate food-seeking behavior. Elife. 2018;7: 1–35. PMID: 29547121
56. Wise RA. Role of brain dopamine in food reward and reinforcement. Philos Trans R Soc Lond B: Biol Sci. 2006;361: 1149–1158. PMID: 16874930
57. Szczypka MS, Rainey MA, Kim DS, Alaynick WA, Marck BT, Matsumoto AM, et al. Feeding behavior in dopamine-deficient mice. Proc Natl Acad Sci U S A. 1999;96: 12138–12143. PMID: 10518589
58. Boekhoudt L, Roelofs TJM, De Jong JW, De Leeuw AE, Luijendijk MCM, Wolterink-Donselaar IG, et al. Does activation of midbrain dopamine neurons promote or reduce feeding? Int J Obes. 2017;41: 1131–1140. PMID: 28321131

736 59. Karam CS, Jones SK, Javitch JA. Come Fly with Me: An overview of dopamine receptors
737 in *Drosophila melanogaster*. Basic Clin Pharmacol Toxicol. 2020; 126: 56–65.
738 PMID: 31219669
739 60. Kleinridders A, Pothos EN. Impact of Brain Insulin Signaling on Dopamine Function, Food
740 Intake, Reward, and Emotional Behavior. Curr Nutr Rep. 2019;8: 83–91. PMID: 3100179
741 61. Fiory F, Perruolo G, Cimmino I, Cabaro S, Pignalosa FC, Miele C, et al. The Relevance
742 of Insulin Action in the Dopaminergic System. Front Neurosci. 2019;13. PMID: 31474827
743 62. Tavares G, Martins FatimaO, Melo BernardeteF, Matafome P, Conde Silvia v. Peripheral
744 Dopamine Directly Acts on Insulin-Sensitive Tissues to Regulate Insulin Signaling and
745 Metabolic Function. Front Pharmacol. 2021;12. PMID: 34566639
746 63. Stouffer MA, Woods CA, Patel JC, Lee CR, Witkovsky P, Bao L, et al. Insulin enhances
747 striatal dopamine release by activating cholinergic interneurons and thereby signals
748 reward. Nat Commun. 2015;6: 8543. PMID: 26503322
749 64. Labouèbe G, Liu S, Dias C, Zou H, Wong JCY, Karunakaran S, et al. Insulin induces long-
750 term depression of ventral tegmental area dopamine neurons via endocannabinoids. Nat
751 Neurosci. 2013;16: 300–308. PMID: 23354329
752 65. Li Y, Ren L, Fu H, Yang B, Tian J, Li Q, et al. Crosstalk between dopamine and insulin
753 signaling in growth control of the oyster. Gen Comp Endocrinol. 2021;313: 113895.
754 PMID: 34480943
755 66. Nash AI. Crosstalk between insulin and dopamine signaling: A basis for the metabolic
756 effects of antipsychotic drugs. J Chem Neuroanat. 2017;83–84: 59–68. PMID: 27480675
757 67. Volkow ND, Wang GJ, Baler RD. Reward, dopamine and the control of food intake:
758 Implications for obesity. Trends Cogn Sci. 2011;15: 37–46. PMID: 21109477
759 68. Wang GJ, Geliebter A, Volkow ND, Telang FW, Logan J, Jayne MC, et al. Enhanced
760 striatal dopamine release during food stimulation in binge eating disorder. Obesity (Silver
761 Spring) 2011;8: 1601–1608. PMID: 21350434
762 69. Joshi R, Venkatesh K, Srinivas R, Nair S, Hasan G. Genetic Dissection of *itpr* Gene
763 Function Reveals a Vital Requirement in Aminergic Cells of Drosophila Larvae. Genetics.
764 2004;166: 225–236. PMID: 15020420
765 70. Pathak T, Agrawal T, Richhariya S, Sadaf X, Hasan XG. Store-Operated Calcium Entry
766 through Orai Is Required for Transcriptional Maturation of the Flight Circuit in Drosophila.
767 2015;35: 13784–13799. PMID: 26446229
768 71. Ashburner, M. (1989) Drosophila. A Laboratory Hand- book. Cold Spring Harbor
769 Laboratory Press, Cold Spring Harbor.
770
771

Figure 1:*STIM^{KO}* larvae exhibit reduced feeding followed by systemic growth arrest.

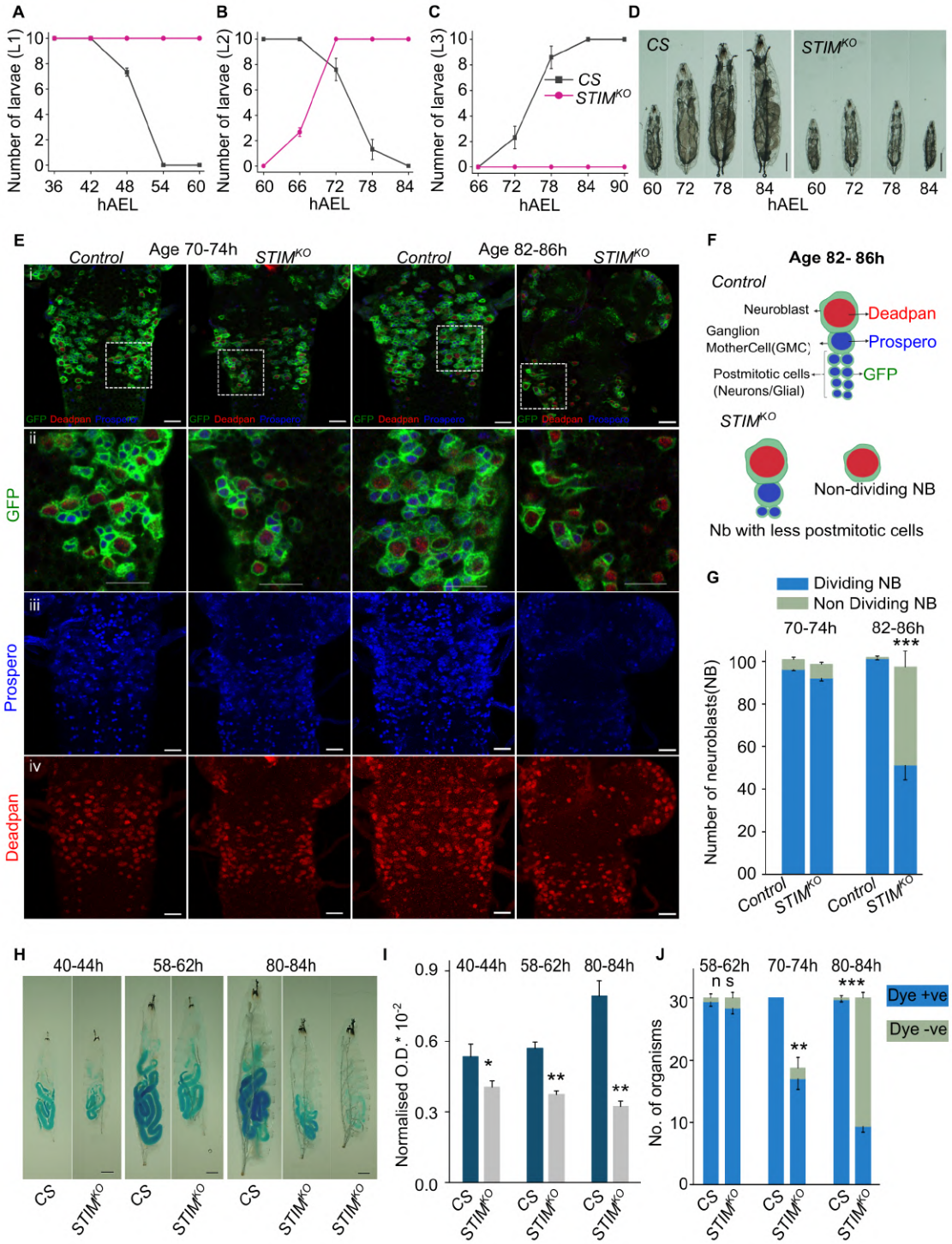

(A-C) Number of 1st instar (L1), 2nd instar (L2) and 3rd instar (L3) larvae from *CS* (grey) and *STIM^{KO}* (red) measured at 6h intervals after egg laying (AEL) at the specified time points (mean ± SEM). Number of sets (N) = 3, number of larvae per replicate (n) = 10.

(D) Representative images of larvae from *CS* and *STIM^{KO}* at the indicated time. Scale bar = 1mm

(E) Representative images of thoracic neuroblasts marked with *Insc>mCD8GFP* (green), a neuroblast marker (anti-Deadpan, red) and a marker for post-mitotic cells (anti-Prospero, blue) from control and $STIM^{KO}$ animals at the indicated ages. Similar images were obtained from four or more animals. Scale bar = 20μm.

(F) Diagrammatic summary of neuroblast proliferation in control and $STIM^{KO}$ animals.

(G) Stack bar graph showing number of dividing neuroblasts to non-dividing neuroblasts. $^{*}P < 0.05$, Student's *t*-test with unequal variances, n = 4 animals from each genotype.

(H) Representative images of dye-fed larvae from *CS* and $STIM^{KO}$ at the indicated times AEL, scale bar = 200μm.

(I) Quantification (mean ± SEM) of ingested blue dye in *CS* and $STIM^{KO}$ larvae at the indicated ages by normalizing optical density (OD) of the dye at 655nm to concentration of protein. Number of feeding plates per time point (N) = 6, number of larvae per plate (n) =10. $^{*}P < 0.05$, Student's *t*-test with unequal variances.

(J) Bar graph showing average number of dye-fed *CS* and $STIM^{KO}$ larvae at the indicated ages (mean ± SEM). Number of feeding plates per time point (N) = 3, number of larvae per plate (n) = 30. $^{*}P < 0.05$, Student's *t*-test with unequal variances.

815 **Figure 2 : Feeding and growth deficits of *STIM*^{KO} larvae arise from central dopaminergic**
816 **neurons**

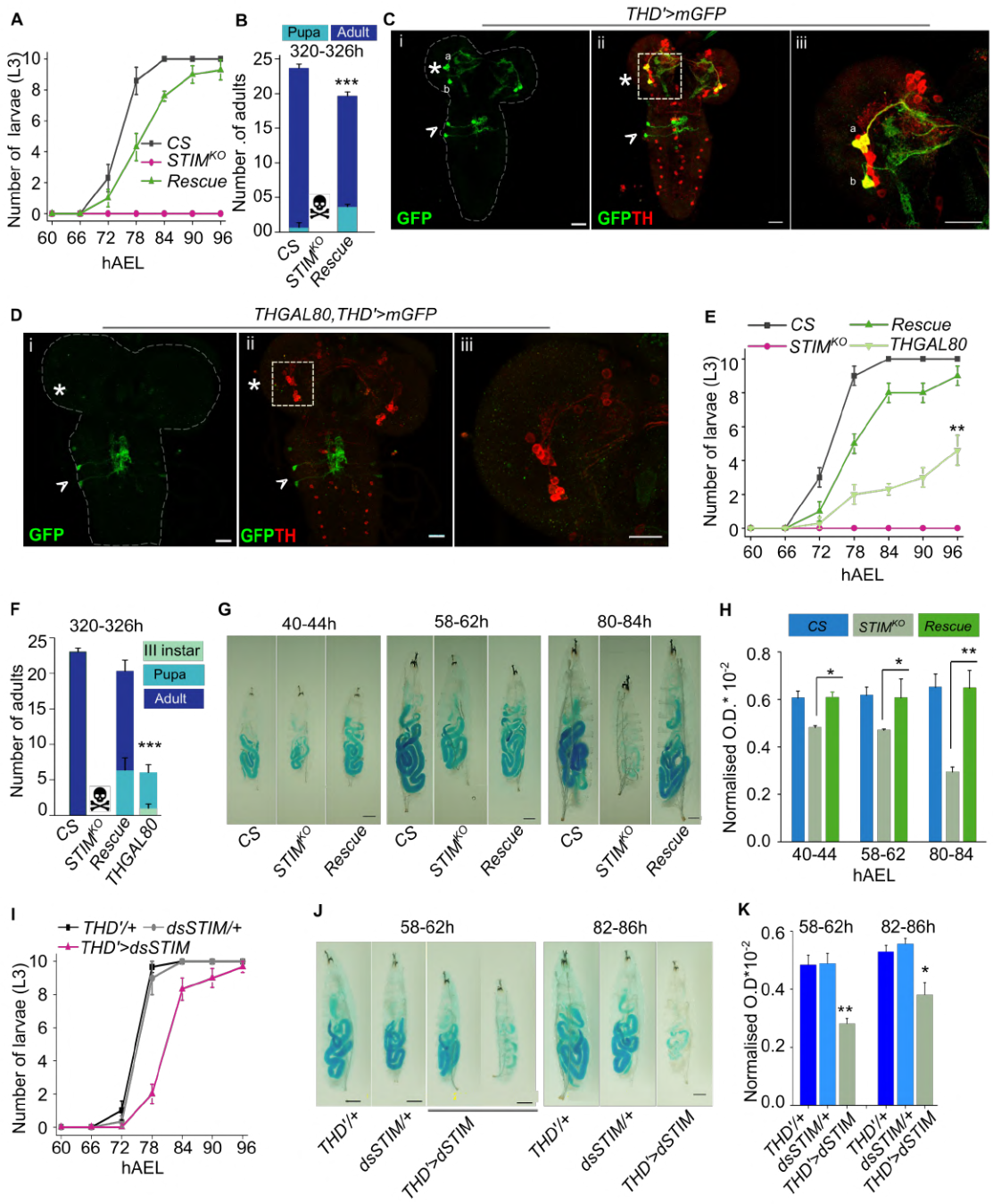

817

818 **(A)** Number (mean ± SEM) of 3rd instar larvae (L3) are restored close to wildtype (CS) levels
819 by expression of *STIM*$^{+}$ in *THD'* cells of *STIM*^{KO} larvae (rescue). Larvae were monitored
820 at 6h intervals from 66h to 96h AEL. Number of sets (N) = 3, number of larvae per set
821 (n) = 10.

822 **(B)** Stack bars with the number of adults (mean ± SEM) that eclosed at 320 to 326h AEL
823 from the indicated genotypes. The genotype of rescue larvae is *STIM^{KO}; THD'>STIM^{+}*.
824 Number of sets (N) = 3, number of organisms per set (n)=25.
825 **(C)** Representative confocal images of the larval brain from animals of the genotype
826 *THD'>mCD8GFP*. Anti-GFP (green) indicates the expression of *THD'GAL4* and anti-TH
827 (red) marks all dopaminergic cells. Asterisks mark TH^{+ve} cells in CNS (i, ii and iii, a and
828 b marks 3 cells of DL1 and 2 cells of DL2 cluster respectively) whereas arrowheads
829 mark non-TH positive cells in ventral ganglia of larval brain (i and ii). Scale bar = 20µm.
830 **(D)** Representative confocal images of the larval brain from animals of the genotype
831 *THGAL80,THD'>mCD8GFP*. *THD'GAL4* driven GFP expression (green) is suppressed
832 in the CNS (asterisks) by *THGAL80* but not in the ventral ganglia (arrowheads). Scale
833 bar = 20µm.
834 **(E)** Line graph shows the number (mean ± SEM) of 3rd instar larvae from *CS, STIM^{KO}*,
835 *STIM^{KO};THD>STIM^{+} and STIM^{KO};THGAL80,THD'>STIM^{+}* at 6h intervals between 60 to
836 96h AEL. Number of sets (N) = 3, number of larvae per set (n) = 10. $^{**}P < 0.01$, Student's
837 *t*-test with unequal variances.
838 **(F)** Stack bar graph showing the number of adults eclosed (mean ± SEM) at 320 to 326h
839 AEL from *CS (*wildtype*), STIM^{KO}* (mutant), *STIM^{KO};THD'>STIM^{+}* (rescue) and
840 *STIM^{KO};THGAL80,THD'>STIM^{+}* (THGAL80 - restrictive rescue) genotypes. Number of
841 sets (N) = 3, number of organisms per set (n) = 25.
842 **(G)** Representative images of dye-fed larvae of *CS, STIM^{KO}* and rescue (*STIM^{KO};*
843 *THD'>STIM^{+}*) genotypes at 40-44h, 58-62h and 80-84h AEL Scale bar = 200µm.
844 **(H)** Bar graph with quantification of ingested food containing a blue dye in larvae of the
845 indicated genotypes (*CS, STIM^{KO}* and rescue) at the indicated developmental times.
846 Mean (mean ± SEM) optical density (655nM) of blue dye in larval lysates after
847 normalizing to larval protein concentration (OD/Protein concentration X 10^{-2}) was
848 obtained from 6 feeding plates (N) each containing 10 larvae (n). $^{*}P<0.05$, Student's *t*-
849 test with unequal variances
850 **(I)** Number of 3r^{d} instar larvae (mean ± SEM) from RNAi knockdown of STIM^{+} in THD'
851 neurons (*THD'>dsSTIM*) along with control genotypes *THD'/+* and *dsSTIM/+* at 6h
852 intervals between 66h to 96h AEL (After Egg laying); Number of sets (N) = 3, number of
853 larvae per set (n) = 10.
854 **(J)** Representative images of dye-fed larvae of the indicated genotypes at 58-62h and 82-
855 86h AEL. Scale bar = 200µm.
856 **(K)** Quantification (mean ± SEM) of blue dye containing ingested food (OD/Protein
857 concentration X 10^{-2}; similar to panel D above) in larvae of the indicated genotypes at

858 58-62h and 82-86h AEL. No. of plates for each time point, (N) = 3, number of larvae per
859 plate (n) = 10. *P<0.05, Student's t-test with unequal variances.
860
861
862 **Figure 3**: **The maintenance of excitability of THD' neurons is important for larval growth.**

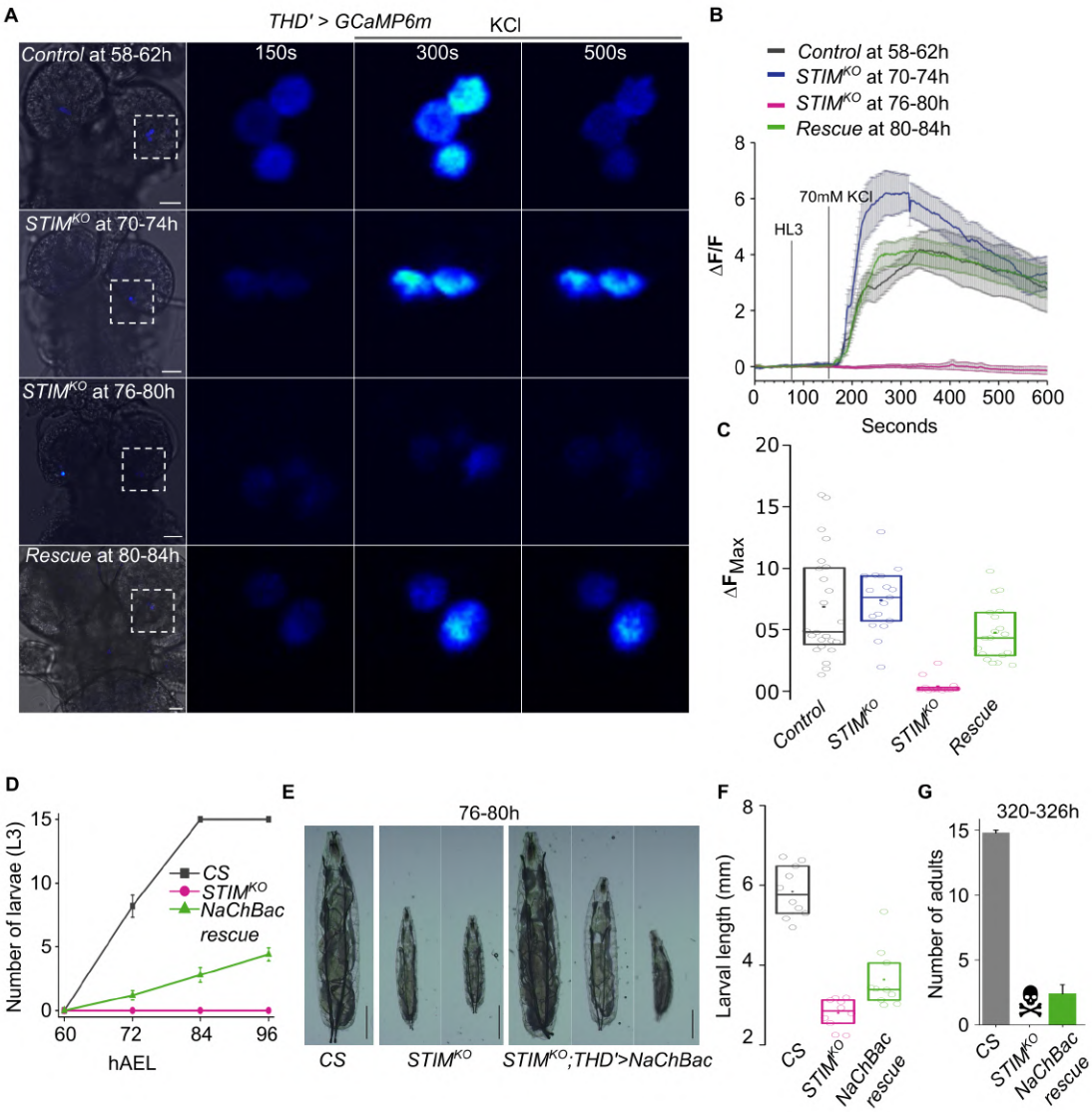

863
864 **(A)** Representative images of the central brain (left panels) indicating the region of focus
865 (boxed), followed by images of THD' cells with Ca^{2+} transients at the indicated time points
866 before and after addition of a depolarizing agent (KCl – 70mM). Ca^{2+} transients were
867 measured by changes in the intensity of GCaMP6m fluorescence in the indicated
868 genotypes. The rescue genotype is *STIM^{KO};THD'>STIM*. Scale bar 20μm
869 **(B)** Changes in GCaMP6m fluorescence (mean ± SEM of ΔF/F) from THD' neurons of the
870 indicated genotypes. Number of brains, (N) ≥ 5, number of cells, (n) ≥ 15.

871 **(C)** Peak intensities of GCaMP6m fluorescence (ΔF) in THD' cells from the indicated
872 genotypes. Box plots show 25th and 75th percentiles, the median (bar), and mean
873 (square) of ΔF of each cell (small circles).
874 **(D)** Number of 3rd instar larvae of *CS, STIM^{KO}* and *STIM^{KO};THD'>NaChBac* genotypes at the
875 indicated times AEL (mean ± SEM). Number of sets (N) = 3, number of larvae per set (n)
876 = 15.
877 **(E)** Representative images of larvae from *CS, STIM^{KO}* and *STIM^{KO}; THD'>NaChBac* at 76-
878 80h AEL, scale bar = 1mm.
879 **(F)** Quantification of larval length from the indicated genotypes. Box plots show the 25th and
880 75th percentiles with median (bar), mean (square) and sizes of individual larvae (circles),
881 n=10.
882 **(G)** Number of adults eclosed at 320h AEL (mean ±_SEM) from wildtype (*CS),* mutant
883 (*STIM^{KO}*) and NaChBac rescue (*STIM^{KO}; THD'>NaChBac*) animals. Numbers were
884 obtained from three experiments (N = 3), number of organisms per experiment, n = 15.
885
886
887
888
889
890
891
892
893
894
895
896
897
898
899
900
901
902
903
904
905
906

907 **Figure 4: STIM is necessary for dopamine release and ER-Ca^{2+} homeostasis**

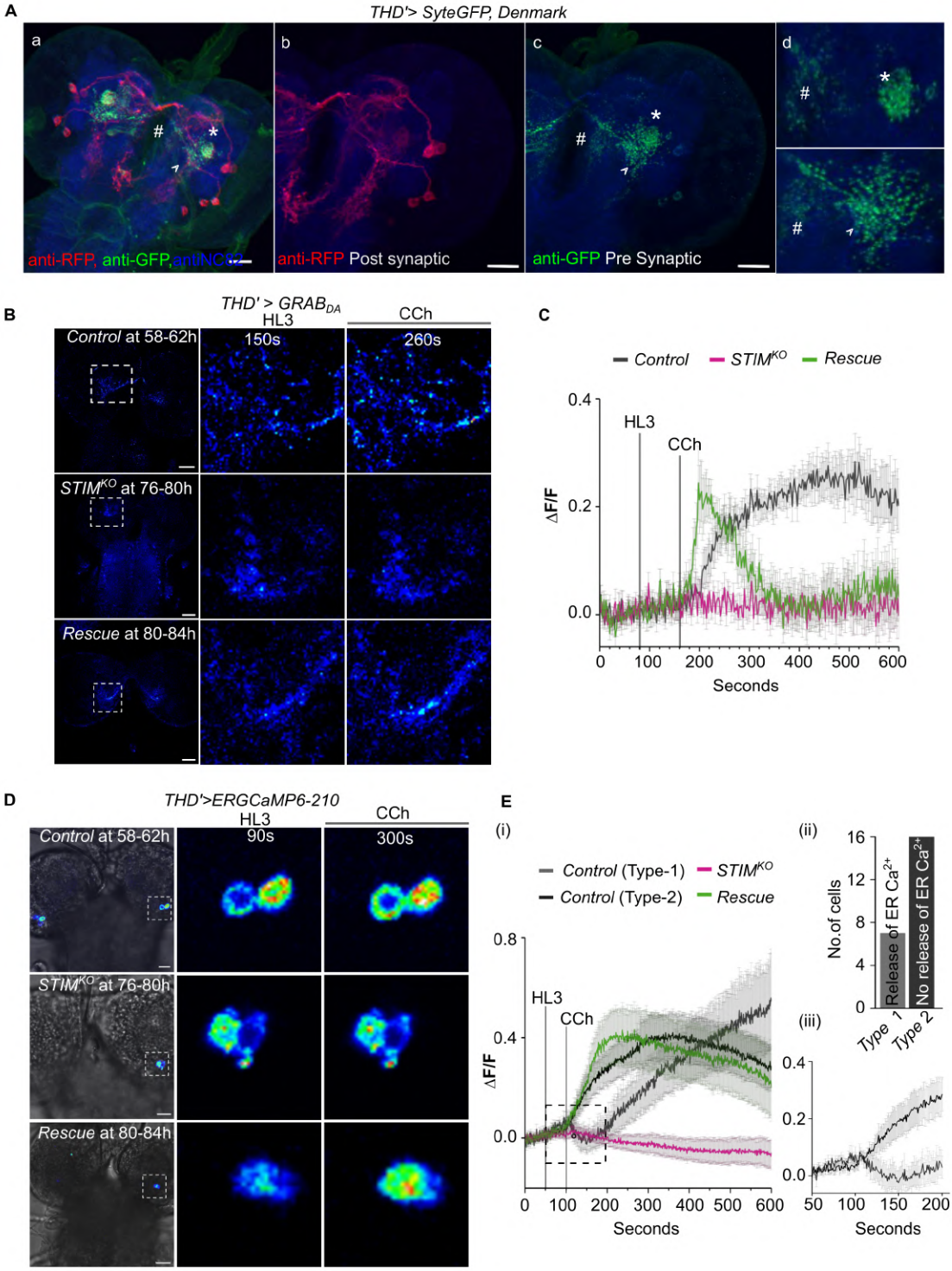

908

909 **(A-D)** Axonal and dendritic projections of THD' neurons visualized by expression of SyteGFP
910 (green) and Denmark (anti-RFP) respectively in a representative brain immunostained
911 for anti-Brp (blue). Panels marked as (d) contain magnified images from (c) of
912 presynaptic terminals (green) located at the centre (asterisk), as branches extruding from
913 the centre (arrowhead) and the brain-gut interaction region (hash) of the CNS.

914 **(E)** Representative images of dopamine release before and after addition of Carbachol
915 (CCh) as measured by changes in intensity of $GRAB_{DA}$ at the presynaptic terminals of
916 THD' neurons in the indicated genotypes. Scale bar = 20mm
917 **(F)** Normalized changes in fluorescence (ΔF/F) of $GRAB_{DA}$ measuring dopamine release
918 from THD' neurons of the indicated genotypes. Traces show the average change in
919 $GRAB_{DA}$ florescence (mean ± SEM of (ΔF/F)) measured from individual presynaptic
920 regions of interest ($\geq$ 10) taken from N $\geq$ 6 brains of each genotype.
921 **(G)** Representative time series images of ER calcium transients as measured by changes in
922 intensity of ER-GCaMP in THD' neurons of the indicated genotypes.
923 **(H)** i) Traces of normalized ER-GCaMP (ΔF/F) responses (mean ± SEM) from THD' neurons
924 of the indicated genotypes. Control (*THD'>ER-GCaMP-210*) Type 1, indicates cells that
925 exhibit ER-Ca^{2+} release upon CCh addition followed by refilling of ER-stores. Control
926 Type 2 indicates cells where ER-Ca^{2+} release was not evident. Rescue indicates
927 $STIM^{KO}$; *THD'>*$STIM^{+}$. For each genotype, number of cells (n) $\geq$ 15 and N $\geq$ 5 brains. (ii)
928 Quantification of control cells that exhibit ER Ca^{2+} release (Type 1) and cells where ER
929 Ca^{2+} release was not observed (Type 2). (iii) Boxed region from (i) enlarged to show ER
930 Ca^{2+} response of Type 1 and Type 2 control cells.
931
932
933
934
935
936
937
938
939
940
941
942
943
944
945
946
947
948
949

950 **Figure 5: Differential regulation of neuropeptidergic cell activity by THD' neurons**

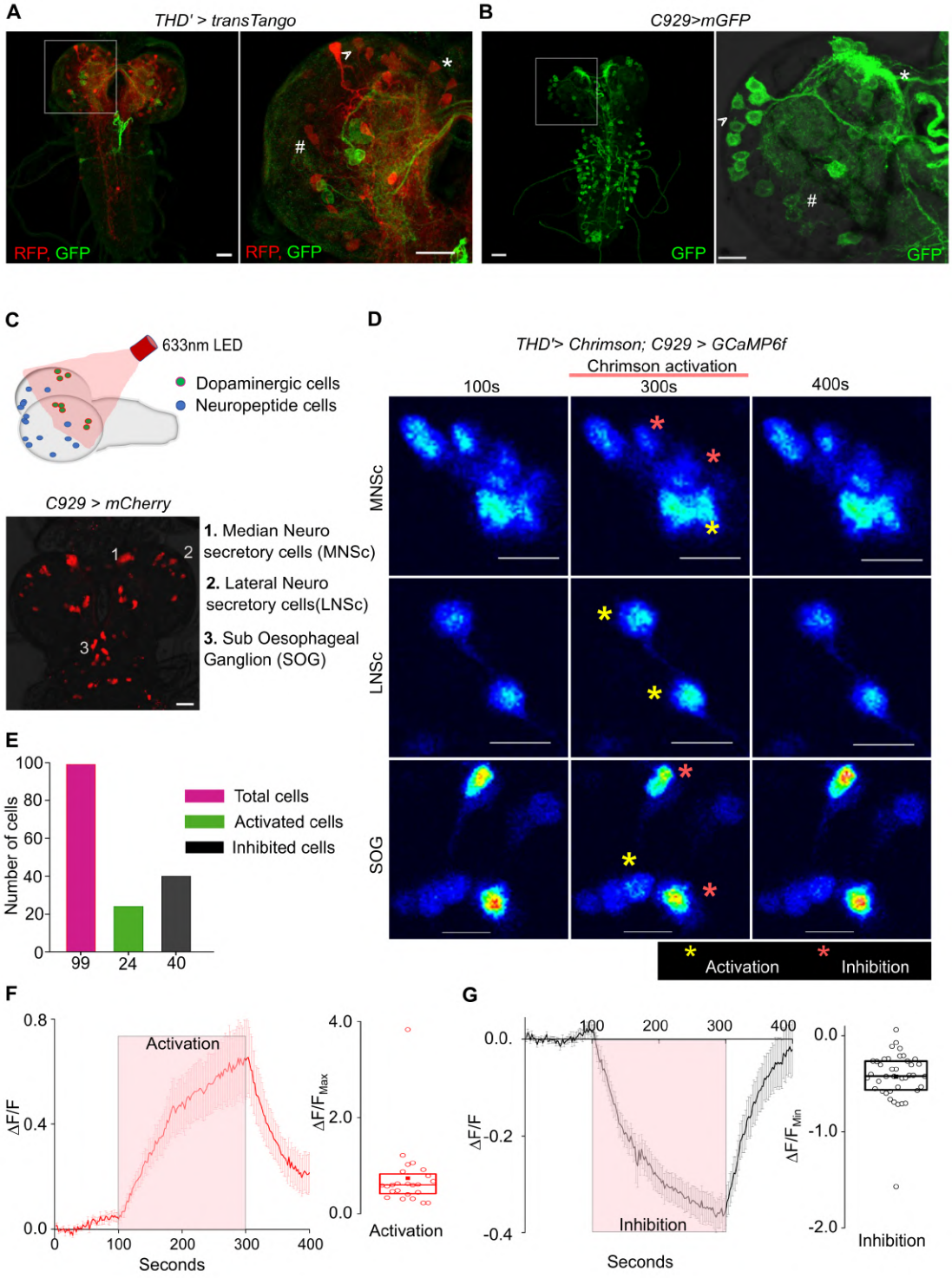

951

952 **(A)** Mapping of neurons that are trans-synaptic to THD' with *THD'>transTANGO* (red) in
953 the larval brain. THD' cells are marked with mGFP (green). The boxed region (left) is
954 shown enlarged on the right. Scale bars = 20μm.

955 **(B)** Peptidergic neurons (green) marked by *C929LexA>LexAopGFP* in the larval brain. The
956 boxed region (left) is shown enlarged on the right. Note similarity to some red cells in
957 A (arrowheads). Scale bars = 20µm
958 **(C)** Pictorial representation of an experimental setup for testing functional connectivity of
959 dopaminergic (THD') and peptidergic (C929) cells in organisms of the genotype
960 *THD'>Chrimson, C929LexA>LexAopGCaMP6m.* The lower panel shows the
961 peptidergic neurons containing regions in which change in Ca^{2+} transients were
962 observed upon activation of THD' cells.
963 **(D)** Ca^{2+} transients in peptidergic Median Neurosecretory cells (MNSc, top), lateral
964 neurosecretory cells (LNSc, middle) and suboesophageal region (SOG, bottom) as
965 measured by the intensity of GCaMP6m before Chrimson activation (100s) and after
966 Chrimson activation (300s and 400s) of THD' cells. Activated cells (red asterisks) and
967 inhibited cells (yellow asterisks) are marked. Scale bar = 20um.
968 **(E)** Quantification of total C929 marked cells from 9 brains that were either optogenetically
969 activated or inhibited.
970 **(F)** Average GCaMP6m responses (mean ± SEM of $\Delta F/F$) across time in C929 marked
971 cells that were activated upon Chrimson activation of THD' neurons at 633nm. The box
972 plot shows 25th and 75th percentiles of peak responses measured by change in
973 GCaMP6m of individual activated peptidergic cells (circles), with the median (bar), and
974 mean (square). n = 24 cells from (N) = 9 brains
975 **(G)** Average GCaMP6m responses (mean ± SEM of $\Delta F/F$) across time in C929 marked
976 cells that were inhibited upon Chrimson activation of THD' neurons at 633nm. The box
977 plot shows 25th and 75th percentiles of peak responses measured by change in
978 GCaMP6m of individual inhibited peptidergic cells (circles), with the median (bar), and
979 mean (square). n = 40 cells from (N) = 9
980
981
982
983
984
985
986
987
988
989
990
991

992 **Figure 6: Developmental expression of insulin-like peptide 3 (ilp3) is regulated by STIM**
993 **in THD' neurons**

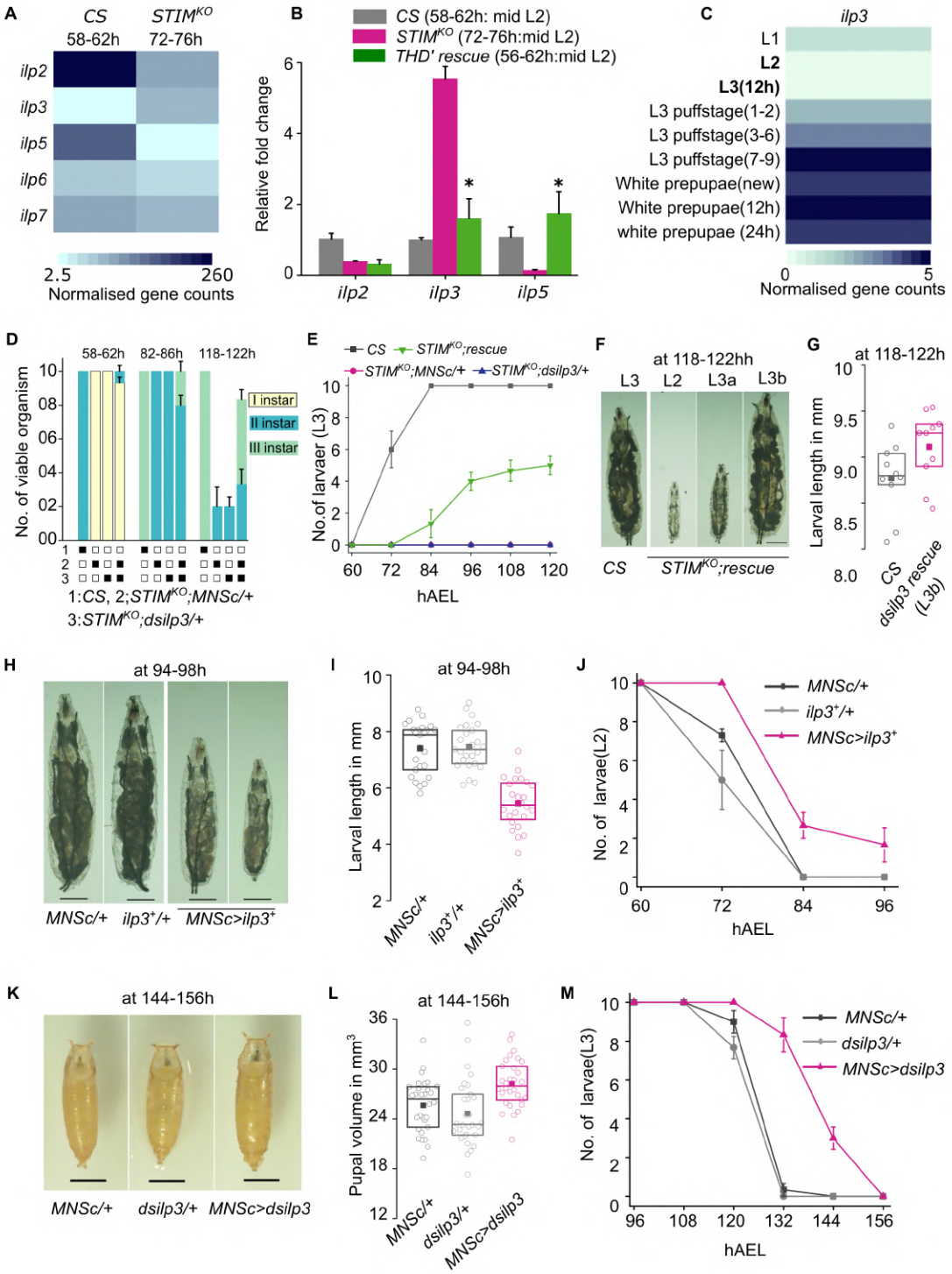

994

995 **(A)** FPKM values obtained for transcripts encoding the indicated insulin like peptides (*ilp*)
996 obtained from an RNAseq experiment performed from *CS* brains (58-62h, mid 2nd instar
997 stage) and *STIM*^{KO} brains (72-76h, mid 2nd instar stage).

998 **(B)** Quantification of *ilp2, ilp3* and *ilp5* transcripts in *STIM*^{KO} brains (pink bar). Expression
999 changes of *ilp3* and *ilp5* transcripts in *STIM*^{KO} brains were rescued upon over-
1000 expression of *STIM*$^{+}$ in THD' neurons (green bar). Transcripts were measured relative
1001 to controls (grey bar). Data show (mean ± SEM) of fold changes of gene expression
1002 (N=3).
1003 **(C)** Heatmap of *ilp3* expression from larval to pupal stages. FPKM values were obtained
1004 from the DGET database https://www.flyrnai.org/tools/dget/web/).
1005 **(D)** Stack bar graph showing the number of viable organisms (mean ± SEM) and their
1006 developmental stage at the specified hours after egg laying for the indicated genotypes.
1007 Number of sets (N) = 3, number of larvae per set (n) = 10
1008 **(E)** Number of 3rd instar larvae of *CS, STIM*^{KO}; *MNScGAL4*, *STIM*^{KO};*UASdsilp3* and
1009 *STIM*^{KO}*;MNSc>dsilp3* genotypes at the indicated times AEL (mean ± SEM). Number of
1010 sets (N) = 3, number of larvae per set (n) = 10.
1011 **(F)** Representative images of larvae from *CS* and *STIM*^{KO}*;MNSc>dsilp3* at 118-122h AEL,
1012 scale bar = 1mm.
1013 **(G)** Quantification of larval length from the indicated genotypes. Box plots show the 25th and
1014 75th percentiles with median (bar), mean (square) and sizes of individual larvae (circles),
1015 n=10.
1016 **(H)** Representative images of larvae from controls (*MNSc/+* and *ilp3*$^{+}$*/+*) and with over-
1017 expression of ilp3 (*MNSc>ilp3*$^{+}$) at 94-98h AEL, scale bar = 1mm.
1018 **(I)** Quantification of larval length from the indicated genotypes. Box plots show the 25th
1019 and 75th percentiles with median (bar), mean (square) and sizes of individual larvae
1020 (circles), n $\geq$24.
1021 **(J)** Number of 2nd instar larvae obtained from the genotypes *MNSc/+, ilp3*$^{+}$*/+* (controls)
1022 *and MNSc>ilp3*$^{+}$ at the indicated time AEL (mean $\pm$ SEM). N = 3 and n = 10.
1023 **(K)** Representative images of pupae from controls (*MNSc/+, dsilp3/+*) and with knock-down
1024 of ilp3 with an RNAi (*MNSc> dsilp3*) at 144-156h AEL, scale bar = 1mm.
1025 **(L)** Quantification of pupal volume from the indicated genotypes. Box plots show the 25th
1026 and 75th percentiles with median (bar), mean (square) and sizes of individual pupa
1027 (circles), n=30
1028 **(M)** Number of 3rd instar larvae of controls (*MNSc/+ and dsilp3/+,* and with knockdown of
1029 ilp3 (*MNSc>dsilp3*) at the indicated times AEL (mean $\pm$ SEM). Number of sets (N) = 3
1030 and number of larvae (n) = 10.
1031
1032
1033
1034

1035 **Supplementary Table 1: FPKM values of selected neuropeptides**

1036

Gene name	*CS*	*STIM*^{KO}	Log2fold	p-value
Ilp2	278.6493	60.52423	-2.207	0.0598
Ilp3	2.516758	30.66396	+3.418	0.0032
Ilp5	130.6938	7.366336	-4.166	0.0024
Ilp6	28.88770	17.25519	-0.755	0.4784
Ilp7	75.89015	54.04743	-0.481	0.6072
CCHa1	52.93767	173.7131	+1.686	0.0446
LK	462.6413	1354.287	+1.546	0.0618
Sifa	116.1298	44.68951	-1.377	0.0232
AstA	53.96644	93.98807	+0.831	0.1853
PDF	98.60125	92.96726	-0.071	0.9157
CCHa2	2.113158	7.342901	+1.599	0.1952
Lst	7.543376	3.688641	+0.864	0.5004
Akh	145.5645	333.8186	+1.190	0.1600
Crz	332.7732	576.2431	+0.787	0.2208
sNPF	2867.630	5488.131	+0.936	0.1941
DH44	301.0334	333.9668	+0.149	0.7875
DSk	53.60334	36.63676	+0.547	0.6110
PTTH	1.878419	1.306375	-0.733	0.6971
FMRFa	206.0697	294.7297	-0.515	0.4000
ITP	23.63023	32.28403	+0.458	0.5496
Rya	0.846811	1.815414	+2.264	0.3660
GPA2	99.54322	183.6279	+0.887	0.3712

1037

1038

1039

1040

1041

1042

1043

1044

1045

1046

1047

1048 # Supplementary figure legends:

1049 **Supplementary figure 1:**

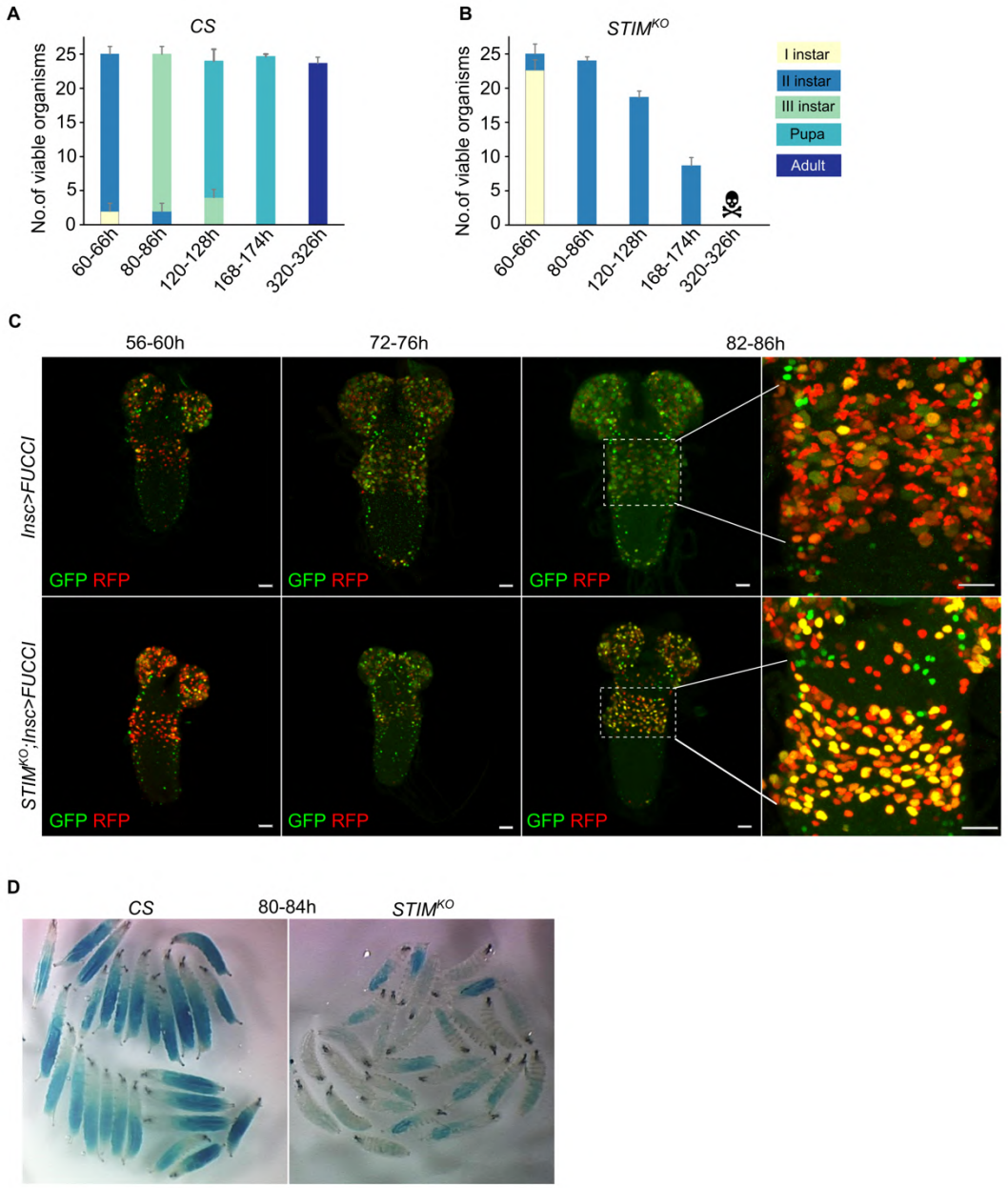

1050

1051

1052 **(A)** Number of viable organisms (mean ± SEM) at the indicated developmental stage after
1053 egg laying. Number of sets (N) = 3, number of organisms per set (n) = 25.

1054 **(B)** Confocal images of larval brains at the indicated time points expressing the FUCCI
1055 marker. Control genotype is *Insc>FUCCI* (top row) and the mutant genotype is *STIM*^{KO};
1056 *Insc>FUCCI* (bottom row). Here late mitosis/G1 phase, S-phase and G2/early mitosis
1057 are marked by green, red, and yellow fluorescent indicators respectively. Scale bar =
1058 20mm; n = 5 larval brains.

1059 **(C)** Representative image of dye-fed larvae from *CS* and *STIM*^{KO} at 80-84h AEL.

1060

1061 **Supplementary figure 2:**

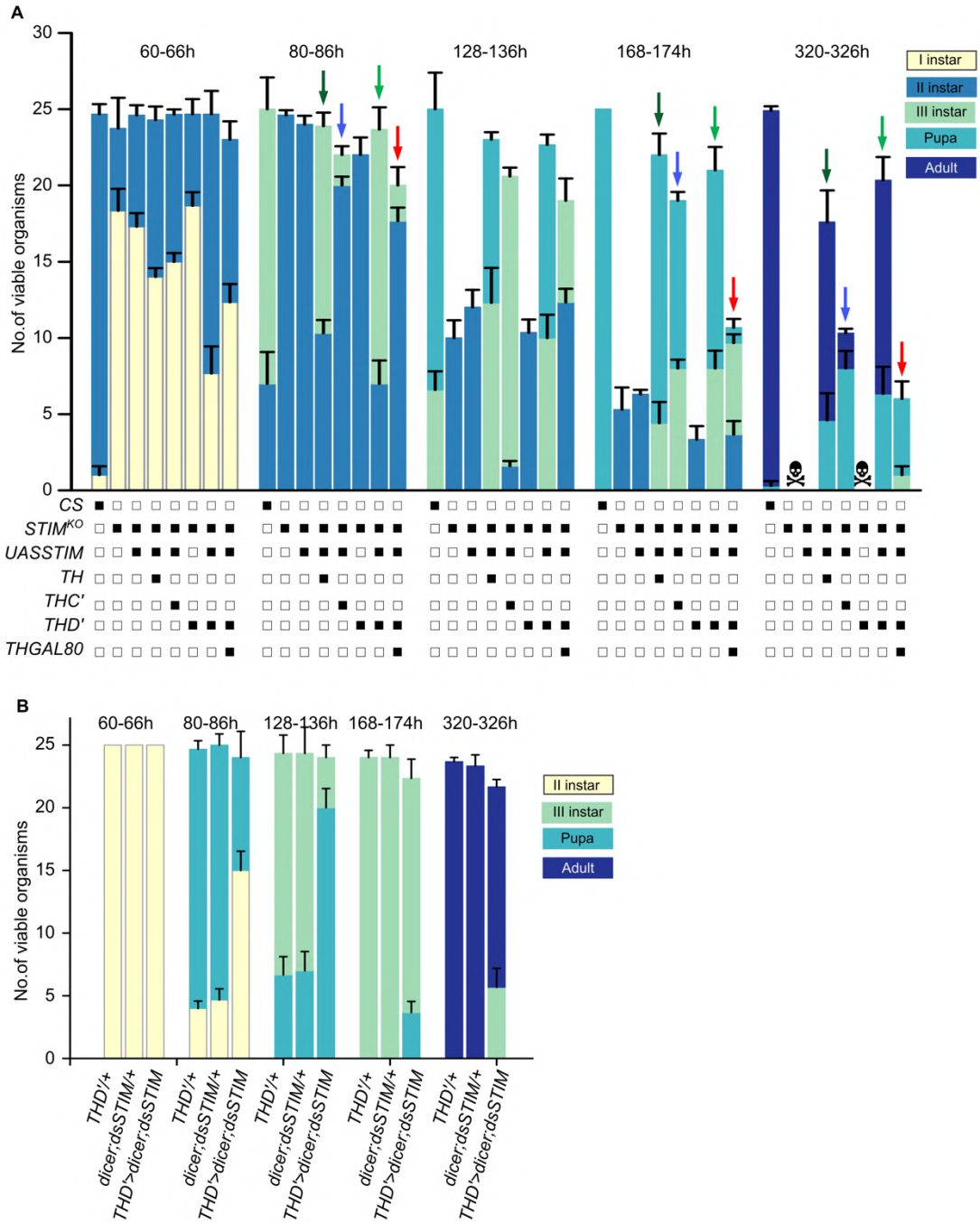

1062

1063 **(A)** Stack bar graph showing the number of viable organisms (mean ± SEM) and their
1064 developmental stage at the specified hours after egg laying for the indicated genotypes.
1065 Coloured arrows mark bars that exhibit rescue of *STIM*^{KO} upon expression of STIM^{+}
1066 driven by *THGAL4* (dark green), *THC'GAL4* (blue), *THD'GAL4* (green) and restricted
1067 rescue in presence *of THGAL80* (red). Number of sets (N) = 3, number of organisms per
1068 set (n) = 25.

1069 **(B)** Stack bar graph showing the number of viable organisms (mean ± SEM) and their
1070 developmental stage at specified hours after egg laying for the indicated genotypes.
1071 Number of sets (N)=3, number of organisms per set (n)=25.
1072
1073 **Supplementary figure 3:**

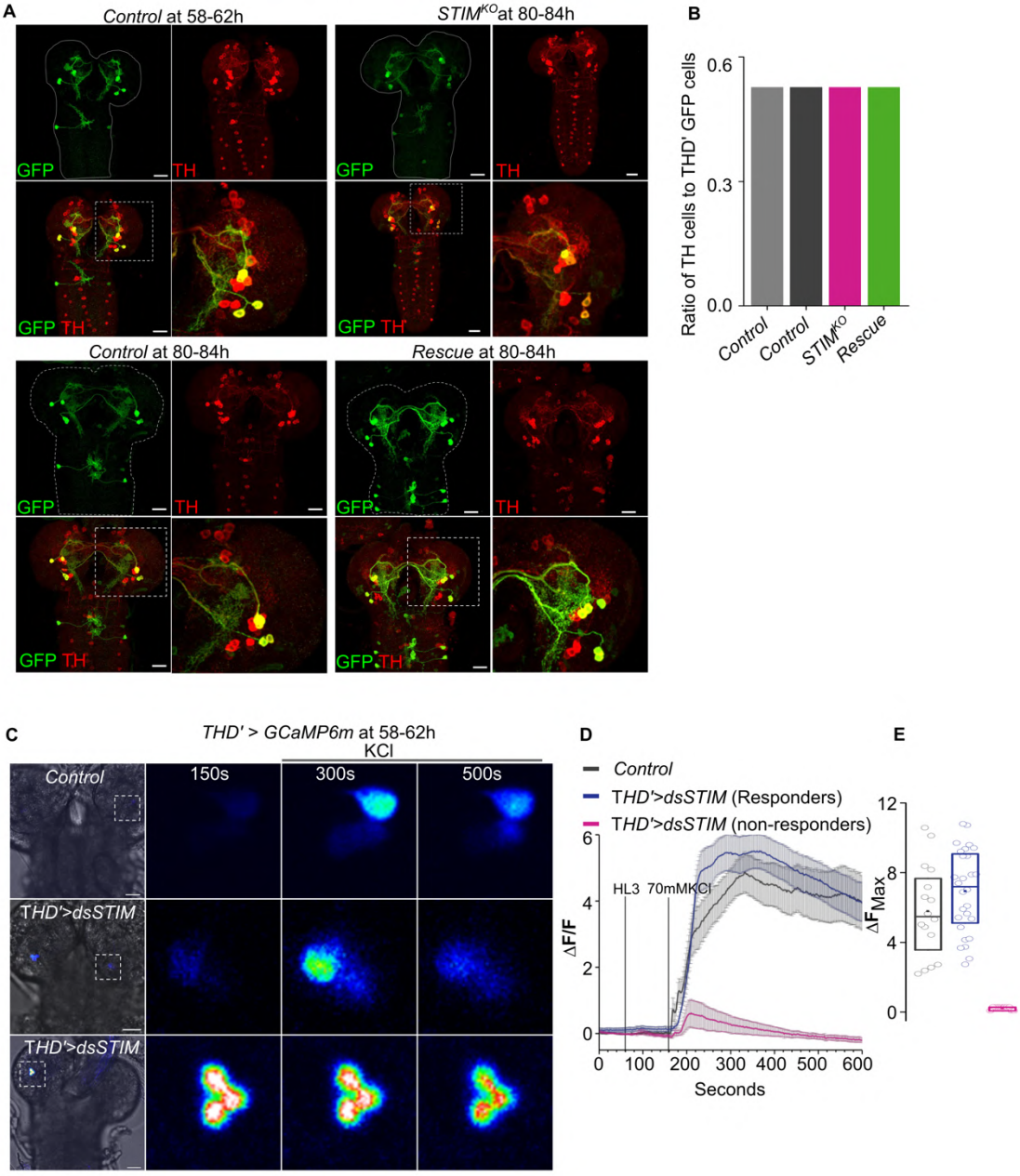

1074
1075
1076 **(A)** Representative confocal images of larval brains showing THD' neurons marked with anti-
1077 GFP (green) and anti-TH (red) from control (*THD'>mCD8GFP*), *STIM^KO* (*STIM^KO*;
1078 *THD'>mCD8GFP)* and rescue (*STIM^KO;THD'>mCD8GFP, STIM^+*) animals at the
1079 indicated developmental time points. Scale bars = 20μm.

(B) Ratio of TH positive cells (red) to THD' cells (green) in the larval CNS of the indicated genotypes. n ≥ 3 brains.

(C) Representative images of the central brain (left panels) indicating the region of focus (boxed), followed by images of THD' cells with Ca^{2+} transients at the indicated time points after addition of a depolarizing agent (KCl, 70mM). Ca^{2+} transients were measured in the indicated genotypes by measuring changes in the intensity of GCaMP6m fluorescence. Scale bar = 20µm

(D) Quantified changes in GCaMP6m fluorescence (mean ± SEM of ΔF/F) from THD' neurons of the indicated genotypes. Number of brains, (N) ≥ 6, number of cells, (n) ≥11.

(E) Peak intensities of GCaMP6m fluorescence (ΔF) in THD' cells from the indicated genotypes. Box plots show 25th and 75th percentiles, the median (bar), and mean (square) of ΔF of each cell (small circles).

Supplementary figure 4:

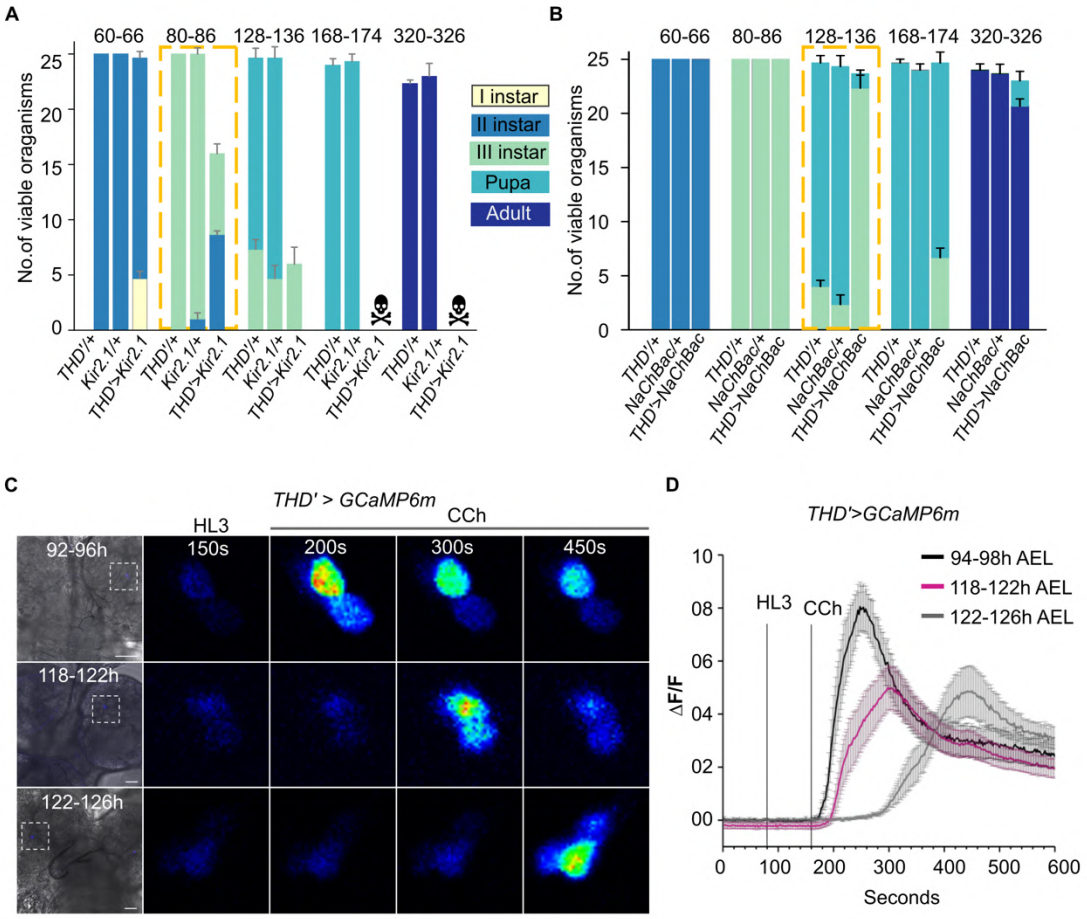

(A) Altered excitability in THD' neurons by expression of either a mammalian inward rectifying potassium channel (Kir2.1) or **(B)** a bacterial sodium channel affects larval

1098 developmental progression. Stack bar graphs show the number of viable organisms
1099 (mean ± SEM) and their developmental stage at the indicated hours after egg laying (top)
1100 for the indicated genotypes. Number of sets (N) = 3, number of organisms per set (n) =
1101 25.

1102 **(C)** Representative images of the central brain (left panels) indicating the region of focus
1103 (boxed), followed by images of THD' cells with Ca^{2+} transients at the indicated time points
1104 after addition of mAChR agonist (CCh 100μM). Ca^{2+} transients were measured in the
1105 indicated genotype by measuring the changes in the intensity of GCaMP6m
1106 fluorescence. Scale bar = 20μm

1107 **(D)** Quantified changes in GCaMP6m fluorescence (mean ± SEM of ΔF/F) from THD'
1108 neurons of the indicated genotypes. Number of brains, (N) ≥ 4, number of cells, (n) ≥12.

1109

1110 **Supplementary figure 5:**

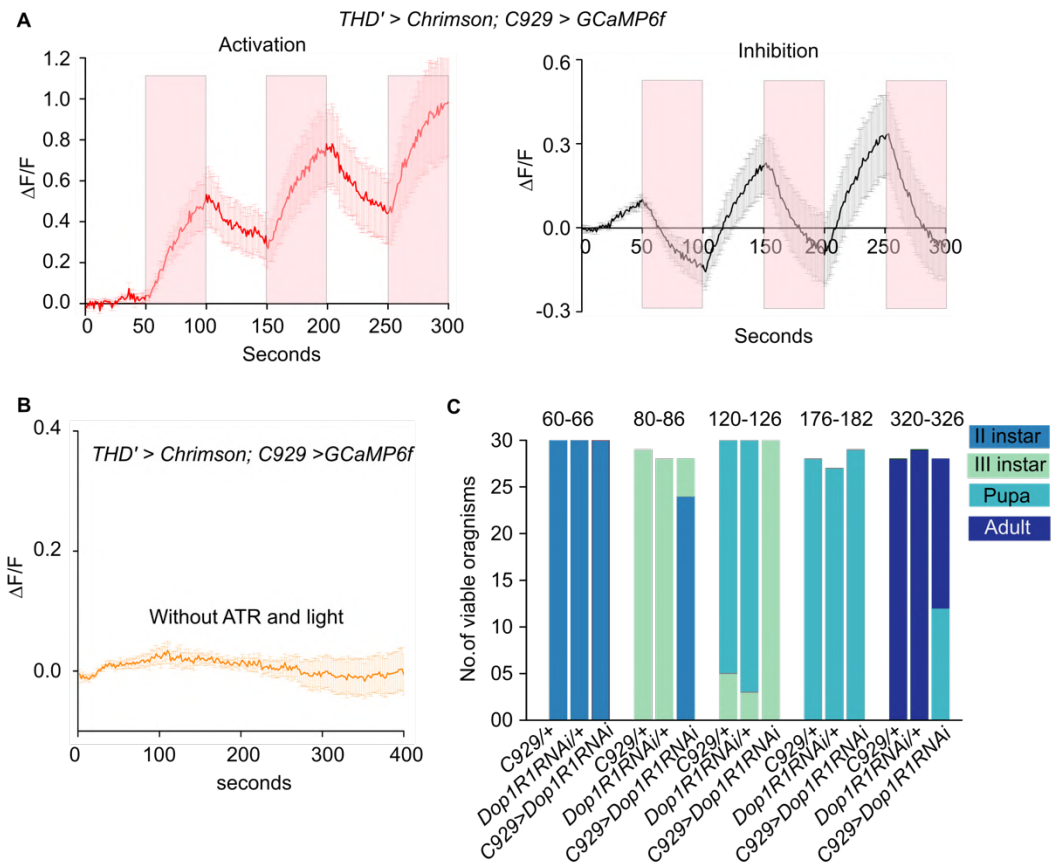

1111

1112 **(A)** Pulsed activation of THD' neurons produce corresponding pulses of activation in certain
1113 peptidergic neurons as evident from their GCaMP6m responses (mean ± SEM). Red
1114 panels indicate the time intervals (50s each) of *THD'>Chrimson* activation. n = 21 cells
1115 from N = 11 brains.

1116 **(B)** Pulsed activation of THD' neurons produce corresponding pulses of inhibition in certain
1117 peptidergic neurons as evident from their GCaMP6m responses (mean ± SEM). Red
1118 panels indicate the time intervals (50s each) of *THD'>Chrimson* activation. n = 19 cells
1119 from N = 9 brains.
1120 **(C)** GCaMP6m responses (mean ± SEM) are absent in C929 cells in the absence of red light
1121 and in larvae that were not fed with All-trans Retinol (ATR). n = 50 cells from N=9 brains.
1122 **(D)** Stack bar graph showing the number of viable organisms and their developmental stage
1123 at the specified hours after egg laying for the indicated genotypes. Number of organisms
1124 per genotype = 30.
1125
1126 **Supplementary figure 6:**

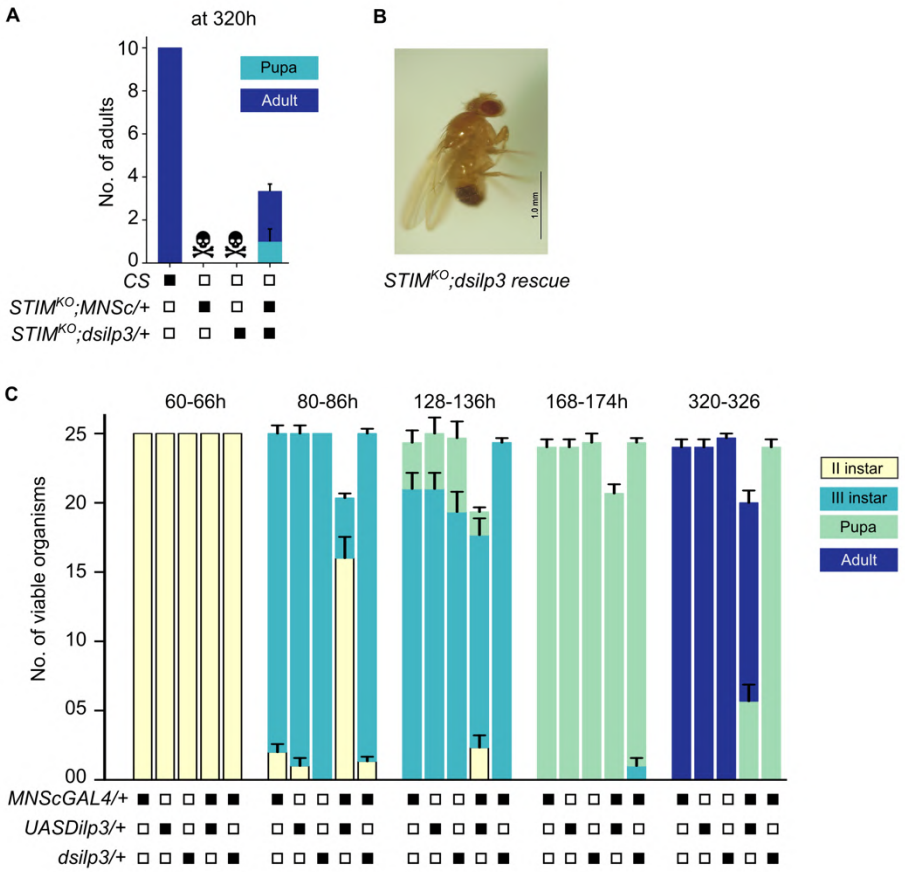

1127
1128 **(A)** Number of adults eclosed at 320h AEL (mean ±_SEM) from *CS, STIM^{KO}; MNSc GAL4,*
1129 *STIM^{KO};UASdsilp3* and *STIM^{KO};MNSc>dsilp3* animals. Numbers were obtained from
1130 three experiments (N = 3), number of organisms per experiment, n = 10
1131 **(B)** Representative image of *STIM^{KO};MNSc>dsilp3* rescued male at 320-326h AEL
1132 **(C)** Stack bar graph showing the number of viable organisms (mean ± SEM) and their
1133 developmental stage at the specified hours after egg laying for the indicated genotypes.

Numbers were obtained from three experiments (N = 3), number of organisms per experiment, n = 25